NUCLEAR STRUCTURE -- EXPERIMENTAL

THE FIRST EXPERIMENT WITH THE S800 SPECTROGRAPH - STUDY OF ^{10}Li

J. A. Caggiano, D. Bazin, B. Blank, W. Benenson, B. S. Davids, B. Sherrill, J. Yurkon, and A. Zeller

INTRODUCTION

The S800 is a large acceptance, high resolution spectrograph that was completed and commissioned in September 1996[1]. The angular acceptance is 20 msr (7°x10°), the momentum acceptance at the focal plane is ± 2.5% and the momentum resolution is 1 in 20,000. In the first experiment with the S800, it was used to study ^{10}Li via the reaction ^{9}Be(^{9}Be,^{8}B)^{10}Li. ^{10}Li is important for 3-body calculations of the halo nucleus ^{11}Li. Several measurements of the states in ^{10}Li have been made, but there is no consensus on its mass or structure[2].

EXPERIMENTAL DETAILS

A primary beam of ^{9}Be (40.1 MeV/u) was transported from the K1200 cyclotron to the target of the S800 spectrograph where it bombarded a 0.94 mg/cm^2 ^{9}Be target. The spectrograph rigidity was set to center the ^{8}B products from the ground state of ^{10}Li in the focal plane. The central angle of the spectrograph was set to 5° to cover angles between 0 and 10°.

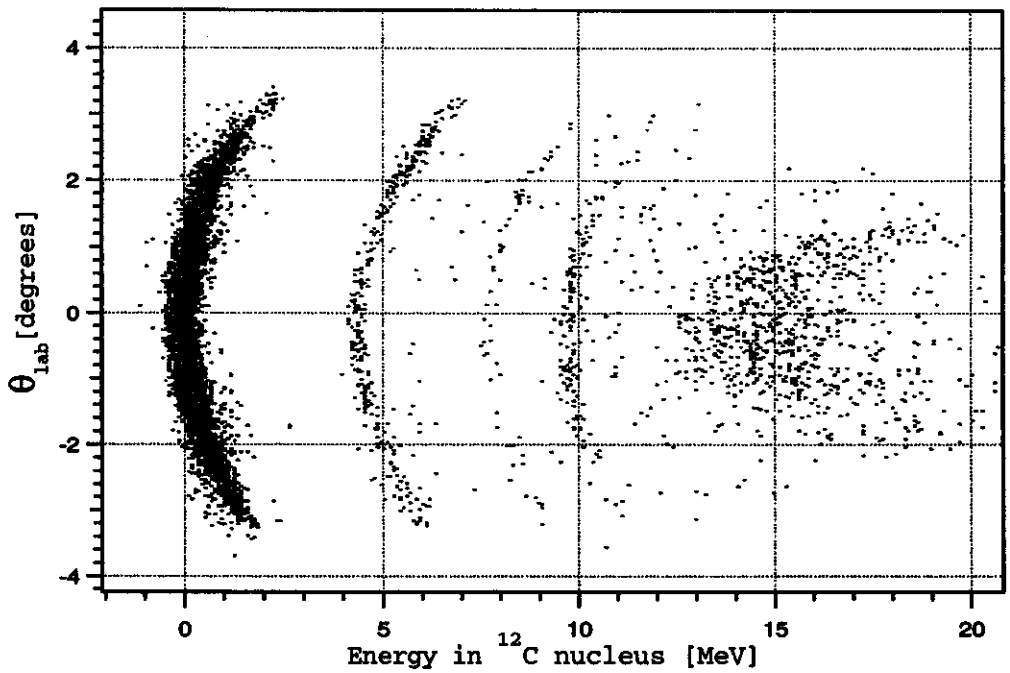

Figure 1: Elastic and inelastic scattering of ^{9}Be beam from ^{12}C target. Theta is the angle in the dispersive direction measured in the focal plane. The ground state and first three excited states of ^{12}C are clearly visible. The parabolic line shapes are indicative of kinematic energy shifts and the spectrograph aberration (x|θ^2).

The detectors consisted of two Cathode Readout Drift Chambers[3] to measure (x,y) coordinates of the particles in the focal plane and in a plane approximately 1.1 meters downstream of the focal plane, and a 5 cm thick plastic scintillator. From the positions in the two detectors, the particle optical angles θ,ϕ

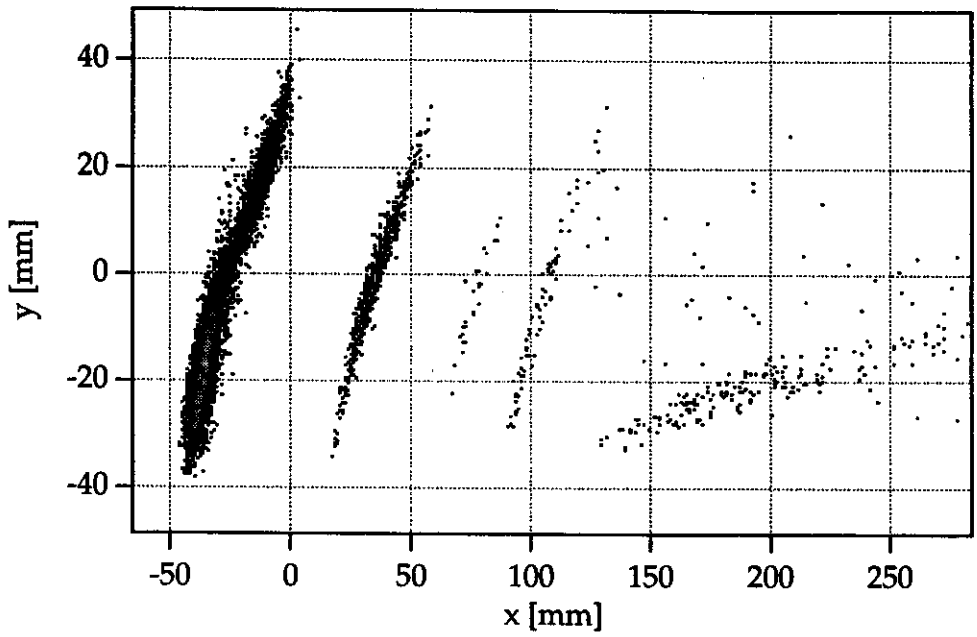

Figure 2: Same reaction as Figure 1, but position is plotted instead. Again the ground state and first three excited states of carbon are clearly visible. The almost horizontal group is scattering from hydrogen in the target backing.

in the focal plane were obtained. The plastic scintillator provides the master gate for the data acquisition electronics and a total energy measurement for particle identification.

Calibration spectra were obtained using elastic and inelastic scattering of the ^{9}Be beam off the ^{12}C target. Figure 1 shows the angle in the dispersive direction at the focal plane, θ, plotted against energy. The parabolic shapes of the lines are a combination of kinematic shift and the spectrograph aberration ($x|\theta^2$). Figure 2 is a view of the first CRDC with a small angular gate. The line shapes are again determined by a combination of kinematic shift and spectrograph aberrations. Figure 3 shows a 1-D projection of the spectra, with a small cut in both angles. The energy resolution demonstrated in this spectrum was 1 in 2500, limited by the solid angle.

The calibration reaction was ^{12}C(^{9}Be,^{8}B)^{13}B because states in ^{13}B surround the expected location of the ground state of ^{10}Li. A 1 mg/cm^2 carbon target and 0.94 mg/cm^2 beryllium target were used as the calibration and reaction targets, respectively. A carbon-backed beryllium target was inserted at the end to obtain simultaneous calibration information.

STATUS

Data analysis is ongoing. Ray-reconstruction will be used to significantly enhance the resolution of the spectrograph. Ray-reconstruction will be done both empirically and using the magnetic field maps obtained for this purpose [6] [7] [8] [9].

A previous measurement using this reaction at 14° had $\leq$30 counts in the ground state region[4]. An on-line measurement of the cross-section at this angle gave 1.1 microbarns/sr for the first peak in the spectrum; there were roughly 10,000 counts in that region. There were no target contaminants present, a problem that plagued Bohlen, et al.[5]. Given these two facts, it is likely that this measurement will shed significant light on the ^{10}Li situation.

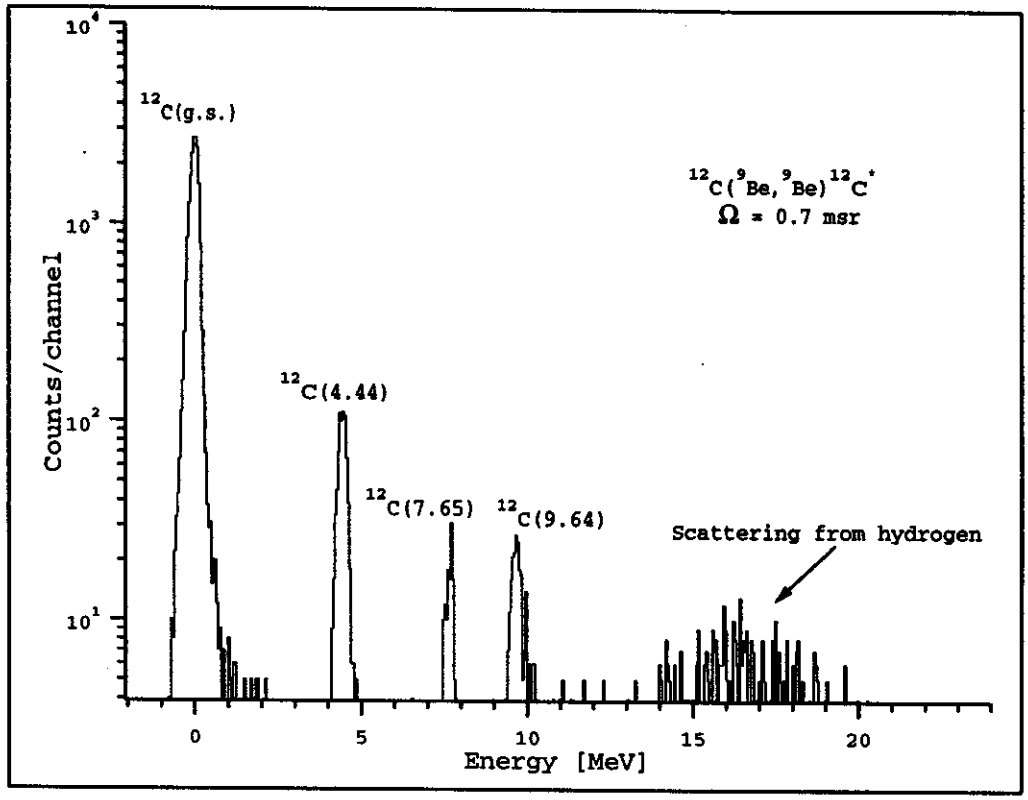

Figure 3: A one dimensional projection of the elastic scattering spectra in Figures 1 and 2. A small angular cut was applied to see the states more clearly.

References

1. A. Zeller, et al., "Completion of the S800 Spectrograph", this annual report.
2. W. Benenson, Nuc. Phys. A588 (1995) 11c-14c.
3. J. Yurkon, et al., "Progress in Focal Plane Detector Development for the S800 Spectrograph", 1994 NSCL Annual Report
4. K. Wilcox, et al., Phys. Letters, 59B(2), 142-144 (1975).
5. H. G. Bohlen, et al., Z. Phys. A 344, 381-393 (1993).
6. J. Caggiano et al., "Automated Data Acquisition System for S800 Dipole Magnetic Field Mapping",1995 NSCL Annual Report.
7. J. Caggiano et al., "Data Analysis Techniques for S800 Dipole Magnetic Field Maps",1995 NSCL Annual Report.
8. J. Caggiano et al., "S800 Spectrograph Dipole Mapping",this annual report.
9. B. Zhang et al., "S800 Quadrupole Mapping", this annual report.

COULOMB EXCITATION OF THE ONE NEUTRON HALO NUCLEUS ^{11}Be

M. Fauerbach, M.J. Chromik, T. Glasmacher, P.G. Hansen, R.W. Ibbotson, D.J. Morrissey, H. Scheit, P. Thirolf, and M. Thoennessen

The nucleus ^{11}Be has only two bound states, the $1/2^+$ ground state and the $1/2^-$ excited state, both neutron halo states with root-mean-square radii of approximately 7 fm. Millener *et al.* [1], who were the first to realize the special character of this system, measured the lifetime of the excited state with a Doppler-shift technique and found it to be 166(15) fs corresponding to a B(E1) value of 0.116(12) e^2fm^2. This makes it the fastest known E1 transition between bound states in nuclei and suggests ^{11}Be as an attractive test case for Coulomb excitation with a radioactive beam. There is also the possibility that more subtle effects will appear when reduced transition matrix elements from lifetime measurements are compared with the ones deduced from cross sections for inelastic scattering. The Coulomb transition amplitude approaches unity at small impact parameters so that first-order perturbation theory may no longer be valid, and the extended halo wave functions may lead to nuclear excitation even beyond distances normally considered 'safe' in Coulomb excitation experiments. However, the first such experiment [3] in which a ^{11}Be beam bombarded a lead target produced an excitation cross section of 191(26) mb at 43 MeV/nucleon, only 40% of the expected value for pure Coulomb excitation at this energy. This reduction is well beyond what could be expected from higher-order effects that are predicted to be on the order of 10-20% [3, 4, 5, 6]. We report here a new experiment in which both heavy and light targets (lead, gold, carbon and beryllium) were studied in order to obtain additional information on the various contributions to the cross section that scale differently with Z and A.

The secondary ^{11}Be beam with an energy of 59.7 MeV/nucleon was produced using a 80 MeV/nucleon ^{18}O primary beam. The ^{11}Be fragment beam was then transported to the N3 vault, where it impinged on the secondary target which was surrounded by an array of 38 position sensitive NaI(Tl) detectors arranged in three concentric rings around the target and shielded from background photons by 16.5 cm thick walls of low-background lead. In this series of measurements four different secondary targets (^{208}Pb (80 mg/cm^2), ^{197}Au (533 mg/cm^2), ^{nat}C (411 mg/cm^2), ^{9}Be (195 mg/cm^2)) were used to excite the projectiles. A detailed description of the experimental setup can be found in [10].

The Doppler-corrected γ-ray energy spectra, recorded under the condition that a ^{11}Be fragment was detected in the zero degree-detector, are shown in Fig. 1. The photopeaks centered around a γ-ray energy of 320 keV in the projectile frame ($\beta \approx 0.34$) – corresponding to the $1/2^- \rightarrow 1/2^+$ transition in the ^{11}Be projectile – are clearly visible for all targets. The low energy of the γ-ray leads to a substantial absorption in the thick gold target, which was calculated using the absorption coefficients of Ref. [12] taking the energy dependence of the absorption coefficient caused by the Doppler-shift into account. (The angular distribution is isotropic in the projectile rest frame for a $\frac{1}{2}^- \rightarrow \frac{1}{2}^+$ transition.) The calculated transmission probabilities are for the gold target 57%, for the ^{208}Pb target 87%, for the carbon target 84%, and for the beryllium target 92% .

The $\frac{1}{2}^+ \rightarrow \frac{1}{2}^-$ excitation cross sections given in Table 1 were obtained from the gamma-ray yields normalized to the number of beam particles detected in the zero-degree detector. These, in principle, reflect the acceptance of the experiment, but are most likely close to the total cross sections for this channel. Noting that a description in terms of a classical impact parameter is valid at the energies discussed here, we find for the two heavy targets (gold and lead) that the Rutherford trajectories correspond to distances

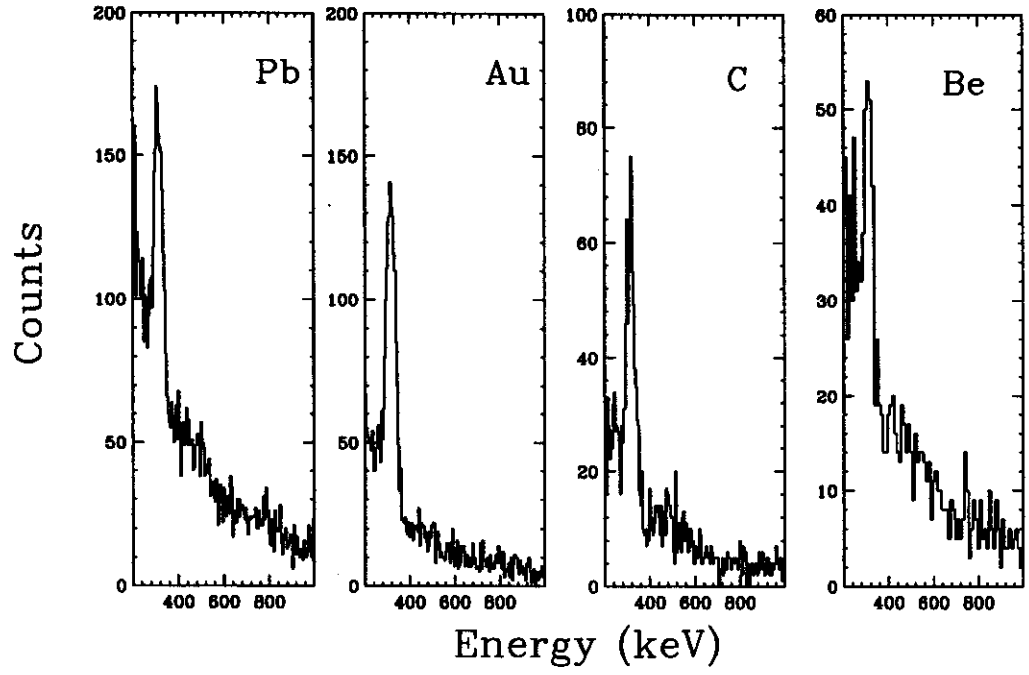

Figure 1: Comparison of B(E1) values obtained from three measurements of the lifetime of the 320 keV excited state [1,2] and from the three Coulomb excitation experiments carried out at 57-60 (this experiment), 64 MeV/nucleon [7], and 43 MeV/nucleon [16], respectively, from left to right. The solid symbols represent the present data and the error bars include both statistical and systematic errors.

of closest approach of approximately 11.5 fm. This distance is about 2 fm larger than the sum of the target - core nuclear interaction radii and hence corresponds to a situation where nuclear contributions are normally considered to be small. (This, of course, is the rationale behind the chosen dimension of the zero-degree detector.) However, since the halo wave function of ^{11}Be extends beyond the nuclear surface with a characteristic decay length of 7 fm, appreciable nuclear contributions are possible. This is *a fortiori* true for the light targets, beryllium and carbon, for which there is no direct selection of the impact parameter and for which scattering through larger angles cannot be excluded directly. We assume in the following that this effect is small because collisions between the light targets and the ^{10}Be core, both fragile systems, will lead to fragmentation at distances smaller than the sum of the two interaction radii.

We discuss the results of Table I by proceeding from the main effects towards the smaller and more uncertain contributions. For the heavy targets (gold and lead) the dominant contribution clearly is Coulomb excitation. The relativistic theory of Winther and Alder [13], leading to the B(E1) values given in Table 1, is based on first-order perturbation theory in an semiclassical model which includes a lowest-order correction for the deviation from a straight-line trajectory. This correction amounts to less than 2% of the cross section for the heavy targets, so the calculation should be very reliable. In Fig. 2 the B(E1) values are compared with those from previous measurements of the lifetime [2, 1] and of inelastic excitation cross sections [3, 7]. Our results confirm the recent RIKEN result and agree, at least marginally, with the lifetime measurements and seem to exclude the small B(E1) value from the GANIL experiment. Below we shall return to the question whether Coulomb contributions beyond perturbation theory and nuclear interactions might affect the measured cross sections.

The nuclear interaction becomes much more important for the two light targets (beryllium and carbon) as the Coulomb and nuclear contributions scale approximately as Z^2 and $A^{1/3}$, respectively. The

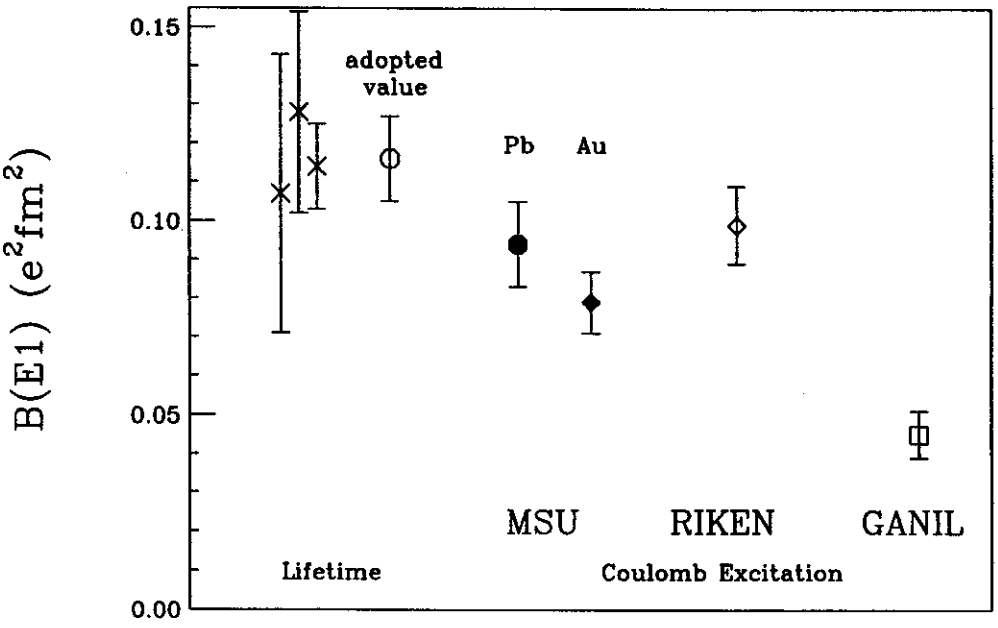

Figure 2: Gamma energy spectra for 60 MeV/nucleon ^{11}Be beams incident on four different targets. The events have been corrected for the Doppler shift. The 320 keV gamma ray corresponding to the $\frac{1}{2}^- \rightarrow \frac{1}{2}^+$ transition in ^{11}Be is clearly seen in all cases. The bin size for the beryllium target is 10 keV, whereas that for the other spectra is 5 keV.

B(E1) values found from the heavy targets lead to Coulomb cross sections of 0.9 mb (beryllium) and 1.9 mb (carbon). An estimate of the nuclear cross sections was obtained with an eikonal model similar to that of reference [15], which used Woods-Saxon single-particle wave functions to obtain the transition amplitude from the $s_{1/2}$ to the $p_{1/2}$ state. With an additional factor of 0.7 to correct for the single-particle occupancy of the two states we arrive at an estimate of approximately 2.5 mb for the two nuclear cross sections. (This method is not valid for the heavy targets, which have a diameter much larger than the decay length of the halo wave function.) Thus, with possible interference effects neglected, the total estimates for the excitation cross sections on carbon and beryllium come out to be 3.4 mb and 4.4 mb, respectively, in qualitative agreement with the measured values of 1.7 mb and 4.0 mb.

As an aside one can compare the relative sizes of the Coulomb and nuclear cross sections for excitations to the bound state discussed here with the excitation of ^{11}Be to continuum states of n+^{10}Be in reactions with a Be target. There (albeit at a slightly different energy of 41 MeV/nucleon) the calculated Coulomb cross section [16] is about 7 mb to the continuum p states and the corresponding nuclear cross section is relatively much larger, about 180 mb in agreement with the experiment [16].

The question is now whether the cross sections for the two heavy targets are influenced by mechanisms other than the first-order Coulomb excitation used for translating the cross sections into the reduced E1 transition probability given in Table 1. This problem has been considered by several authors [3, 4, 6] in connection with the GANIL experiment with the small reported cross section at 43 MeV/nucleon [3]. One possible contribution would be higher-order electromagnetic effects that couple the excited state to the continuum. A coupled-channels calculation by Bertulani *et al.* [6] found that this leads to a 4% reduction in the cross section. Another method is to evaluate the transition probability in the sudden

Target	Thickness [mg/cm^2]	Beam energy [MeV/nucleon]	$\sigma(\theta_{lab} < 3.8°)$ [mb]	B(E1) [e^{2}fm^2]
^{208}Pb	80	59.4	304±10±33	0.094(11)
^{197}Au	533	57.6	244±7±24	0.079(8)
^{nat}C	411	56.7	4.0±0.2±0.5	
^{9}Be	195	58.4	1.7±0.2±0.4	

Table 1: Measured cross sections for ^{11}Be with a scattering angle of less than 3.8° in the laboratory frame, with statistical and systematic errors, the latter arising mainly from the efficiency calibration and the absorption corrections. The beam energy refers to the mid-plane of the target.

approximation, which allows the excitation amplitude to be evaluated to all orders. Comparison of this result with that obtained with the corresponding first order term gives the magnitudes of the reduction of the cross section, which were found to be 6-11% by Typel and Baur [4] and 8% by Anne *et al.* [3]. The effects should decrease with increasing beam energy. Nuclear interactions were found to be very small in a model [6] that considered collective monopole and quadrupole excitation modes, but the main effect is presumably the nuclear interaction of the halo with the target, which has a strong dipole component. An evaluation in a model [3] based on the interaction of a black disc with the halo wave function suggested another reduction by 8%. All the estimates are consistent with a 10%-20% reduction in the effective B(E1) value at 43 MeV/nucleon. The higher-order Coulomb corrections are expected to decrease with increasing beam energy.

At the larger energy of this experiment the ratio of the weighted average of B(E1) values from the three Coulomb excitation measurements carried out at the same energy (and leaving out the result of [3]) to the average obtained from the lifetime measurements is 0.77±0.09. Although this is suggestive of a bigger effect than calculated, the result is consistent with unity. More precise experiments that can differentiate between first-order Coulomb effects and other contributions are required to elucidate the importance of the latter. The results for the light targets should help to assess the non-Coulomb contributions to the cross section.

References

1. D.J. Millener, J.W. Olness, E.K. Warburton, and S.S. Hanna, Phys. Rev C28 (1983) 497.
2. S.S. Hanna, K. Nagatani, W.R. Harris, and J.W. Olness, Phys. Rev. C3 (1971) 2198.
3. R. Anne *et al.*, Z. Phys. A352 (1995) 397.
4. S. Typel and G. Baur, Phys. Let. B 356 (1995) 186.
5. T. Kido, K. Yabana, and Y. Suzuki, Phys. Rev C53 (1996) 2296.
6. C.A. Bertulani, L.F. Canto, and M.S. Hussein, Phys. Lett. B 353 (1995) 413.
7. T. Nakamura, T. Motobayashi, Y. Ando, A. Mengoni, T. Nishio, H. Sakurai, S. Shimoura, T. Teranishi, Y. Yanagisawa, and M. Ishihara, Phys. Lett. B 394, 11 (1997).
8. B.M. Sherrill, D.J. Morrissey, J.A. Nolen Jr., and J.A. Winger, Nucl. Instr. Methods B56 (1991) 1106.
9. D. Swan, J. Yurkon, and D.J. Morrissey, Nucl. Instrum. Methods Phys. Res. Sect. A 348 (1994) 314.
10. M. Fauerbach, Ph.D. thesis, Michigan State University 1997, unpublished.
11. T. Glasmacher, P. Thirolf, and H. Scheit, to be published.
12. Table of Isotopes, edited by R.B. Firestone and V.S. Shirley (John Wiley and Sons, Inc., 1996), Vol. II, p. G1.
13. A. Winther and K. Alder, Nucl. Phys. A319 518 (1979).
14. I. Tanihata, Prog. Part. Nucl. Phys. 35 505 (1995).
15. P.G. Hansen, Phys. Rev. Lett. 77, 1016 (1996).
16. R. Anne *et al.*, Nucl. Phys. A 575 125 (1994).

THE FIRST EXCITED STATE IN ^{44}S

T. Glasmacher, B.A. Brown, M.J. Chromik, P.D. Cottle[a], M. Fauerbach, R.W. Ibbotson, K.W. Kemper[a], D.J. Morrissey, H. Scheit, D.W. Sklenicka[b] and M. Steiner

We have measured the energy and reduced transition probability $B(E2; 0^+_{g.s.} \rightarrow 2^+)$ of the lowest 2^+ state in the neutron-rich radioactive $N = 28$ isotope ^{44}S. This state was excited with the technique of intermediate-energy Coulomb excitation of a radioactive ^{44}S beam having an intensity of only approximately 15 particles/s. With the present measurement, which indicates that ^{44}S is collective, the chain of even-Z $N = 28$ isotones with measured matrix elements $B(E2; 0^+_{g.s.} \rightarrow 2^+)$ has been extended from iron ($Z = 26$) to sulfur ($Z = 16$), allowing a systematic understanding of the effects of the $N = 28$ major shell closure on the structure of these nuclei. With the sole exception of ^{48}Ca, the $N = 28$ isotones are collective, though generally not as much as ^{44}S.

Intermediate-energy Coulomb excitation [2] of radioactive beams has been used recently to populate low-lying states of ^{38,40,42}S and ^{44,46}Ar [3], as well as states in several $A \leq 14$ nuclei [4] and ^{32}Mg [5]. The work reported here was performed at the National Superconducting Cyclotron Laboratory at Michigan State University. A primary beam of $^{48}Ca^{12+}$ at an energy of 70 MeV/nucleon and an intensity of 25 *particle*-nA was produced with the NSCL room temperature electron cyclotron resonance ion source and the K1200 cyclotron. The secondary ^{44}S beam was obtained via projectile fragmentation in a 379 mg/cm^2 ^{9}Be primary target located at the mid-acceptance target position of the A1200 fragment separator [6]. A thin degrader (10 mg/cm^2 carbon) was placed at the second intermediate dispersive image of the A1200 to reduce the number of light fragments that reach the A1200 focal plane and subsequently the experimental setup. The magnetic field settings of the A1200 fragment separator were optimized for the transmission of ^{44}S. Since the production cross section (four proton stripping) for ^{44}S is very small, its yield at the experimental station was approximately 15 particles/s and accounted for only about 0.4% of the secondary beam fragments which reached the Coulomb excitation target.

Photons were measured in coincidence with the scattered secondary beam particles in an array of 38 position sensitive NaI(Tl) detectors. The NaI(Tl) crystals were cylindrical, 18 cm long, 5.75 cm in diameter, enclosed in 0.45 mm thick aluminum shields. The detectors were oriented parallel to the beam direction around a 10.2 cm diameter beam pipe in three concentric rings, and the target was located at the midpoint of the detectors. Photomultiplier tubes were located at both ends of each detector, and the coincident signals from the two photomultiplier tubes were used to determine both the energy of the detected photon and the location of the photon interaction in the detector. Several γ-ray sources (^{22}Na, ^{88}Y, ^{152}Eu and ^{228}Th) were used to establish position-dependent energy calibrations and efficiencies of each detector. The energy resolution of the detectors was typically 8% at 662 keV, and the position resolution was approximately 2 cm, providing an angular resolution of better than 10° for each detected photon. The angular information was used to correct for the large Doppler shifts of the photons emitted from the secondary beam. The entire NaI(Tl) array was shielded from photons produced in the phoswich detector and PPACs, and from room background by a 16.6 cm layer of low-background lead bricks. The time difference between the detection of a photon in the NaI(Tl) detectors and the detection of the secondary beam particle in the phoswich detector was recorded for each event to reduce accidental coincidences.

The photons emitted from secondary beam particles, which had velocities of approximately $v = 0.276c$ (corresponding to a secondary beam energy of 35 MeV/nucleon in the middle of the gold

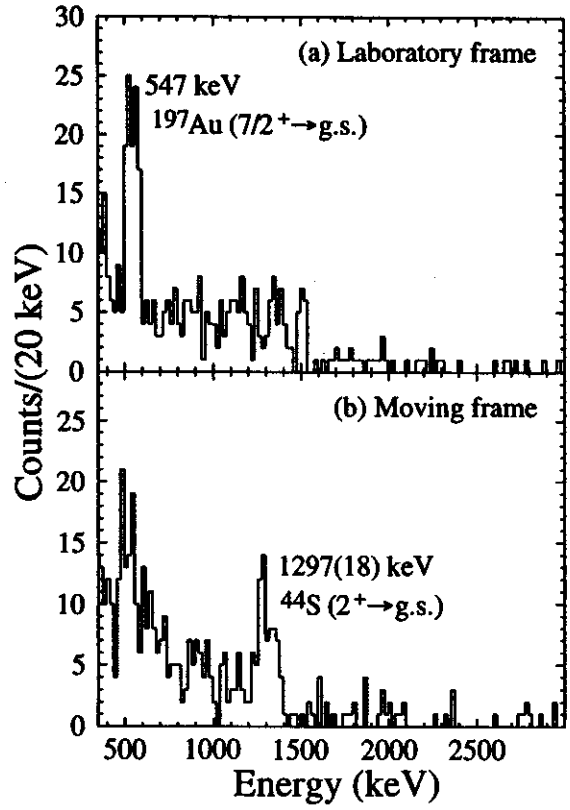

Figure 1: The upper panel (a) contains the photon spectrum in the target frame. The 547 keV ($7/2^+ \rightarrow g.s.$) transition in the ^{197}Au target is visible as a peak, while the ($2^+ \rightarrow g.s.$) transitions in the projectile is very broad. The lower panel (b) contains the same energy spectrum, but Doppler-shifted into the projectile frame ($v = 0.276c$) on an event-by-event basis. The transition corresponding to the first excited state in ^{44}S becomes visible.

target), could be distinguished from those from the ^{197}Au target by their Doppler shifts. Figure 1 shows the γ-ray spectrum in coincidence with ^{44}S in the laboratory-frame (no Doppler correction) and in the Doppler-shifted frame of the projectile. The laboratory-frame spectrum clearly shows a peak from the 547 keV γ-ray corresponding to the $7/2^+ \rightarrow g.s.$ transition in the ^{197}Au target, but no peaks at higher energies. In contrast, the Doppler-shifted spectrum clearly shows a peak at 1297(18) keV corresponding to the first excited state in ^{44}S.

The detector efficiencies were folded with the photon angular distributions [3] in the projectile and target frames to determine the photopeak efficiencies for photons emitted from the excited projectile and target nuclei. By comparing the photon yield of the first excited state in ^{44}S to the yield of the $7/2^+ \rightarrow g.s.$ transition in ^{197}Au we extracted a transition probability in ^{44}S relative to the known electromagnetic transition probability in ^{197}Au [9]. We verified in our data set for the known case of ^{42}S that this method gives identical results to a direct determination of the excitation cross section from the combination of the yield of γ-rays from the 2_1^+ state in ^{42}S, the number of ^{42}S nuclei observed in the phoswich detector, the gold target thickness, and the photon detection efficiency. For ^{44}S we obtained a reduced transition probability of $B(E2; 0_{gs}^+ \rightarrow 2_1^+) = 314(88)$ e^{2}fm^4. The prescription of Raman *et al.* [10] can be used to calculate the reduced quadrupole deformation parameter β_2 from $B(E2; 0_{gs}^+ \rightarrow 2_1^+)$,

$$\beta_2 = 4\pi[B(E2; 0_{gs}^+ \rightarrow 2_1^+)]^{(1/2)}/(3ZR_0^2e), \quad (1)$$

where $R_0 = 1.2A^{1/3}$ fm and $B(E2; 0^+_{gs} \rightarrow 2^+_1)$ is in units of e^2fm^4. For ^{44}S we obtain $|\beta_2^{exp}| = 0.258(36)$.

Naively, the $N = 28$ isotones are expected to be spherical because this neutron number corresponds to a major shell closure. However, the collective $B(E2; 0^+_{g.s.} \rightarrow 2^+_1)$ value in ^{44}S, as well as other collective results found in ^{46}Ar ($\beta_2 = 0.18(2)$) [3], ^{50}Ti ($\beta_2 = 0.17(1)$), ^{52}Cr ($\beta_2 = 0.22(1)$) and ^{54}Fe ($\beta_2 = 0.19(1)$) [11], indicate that the $N = 28$ shell closure is weaker than some of those found in heavier mass regions (for example, the uniformly non-collective nature of the 2^+_1 states of the $N < 82$ even-even Sn isotopes is well known).

A detailed discussion of our experimental results in terms of empirical shell model calculations and a comparison to microscopic calculations has been published [12].

a. Department of Physics, Florida State University, Tallahassee, Florida 32306
b. Permanent address: Drake University, Physics and Astronomy Department, Des Moines, IA 50311

References

1. T.R. Werner et al., Phys. Lett. B 335 (1994) 259; Nucl. Phys. A 597 (1996) 327.
2. A. Winther and K. Alder, Nucl. Phys. A 319 (1979) 518.
3. H. Scheit et al., Phys. Rev. Lett. 77 (1996) 3967.
4. R. Anne et al., Z. Phys. A 352 (1995) 397.
5. T. Motobayashi et al., Phys. Lett. B 346 (1995) 9.
6. B.M. Sherrill et al., Nucl. Instr. Meth. B 56 (1991) 1106.
7. J. Raynal, Computer code ECIS88, unpublished.
8. T. Suomijärvi *et al.*, Nucl. Phys. A 509, 369 (1990).
9. C. Zhou et al., Nucl. Data Sheets 76 (1995) 399.
10. S. Raman et al., Phys. Rev. C 43 (1991) 556.
11. S. Raman et al., At. Data Nucl. Data Tables 36 (1987) 1.
12. T. Glasmacher et al., Phys. Lett. B 395 (1997) 163.

IN-BEAM COULOMB EXCITATION STUDIES OF ^{32,34,36,38}Si

R.W. Ibbotson, T. Glasmacher, M. Chromik[a], P.D. Cottle[b], M. Fauerbach, P.G. Hansen, K. Kemper[b], D. Morrissey, H. Scheit, and M. Thoennessen

Considerable interest in the N=20 Z≈14 nuclei has arisen as a result of the discovery of rapid changes in the structure of these nuclei as a function of Z. The energy levels of ^{34}Si observed so far ($E(2^+)$ = 3.33 MeV) suggest that this nucleus is doubly magic in character as predicted by shell model calculations [1, 2], while the low-lying 2_1^+ state ($E(2^+)$ = 885 keV) and the large value of β_2 [3] in ^{32}Mg suggests that this nucleus is strongly deformed. The best measure of the quadrupole collectivity is not the level energies, but the electromagnetic matrix elements, which can be measured by Coulomb excitation techniques. The availability of high-quality radioactive beams has prompted the application of this technique to β-unstable nuclei, allowing detailed studies of nuclear structure in regions previously inaccessible [3, 4, 5]. We have chosen to use this technique to measure the $B(E2;0^+ \rightarrow 2^+)$ values in a series of neutron-rich silicon isotopes to elucidate the collectivity change in this region.

The ^{32}Si, ^{34}Si and ^{36,38}Si beams were produced in three separate experiments at the NSCL. The ^{32}Si fragments were produced by fragmentation of a 80 MeV/A beam of ^{40}Ar (provided by the K1200 cyclotron) on a 356 mg/cm^2 ^{9}Be target. The resulting fragments were separated (using an achromatic wedge) and identified in the A1200. The resulting beam was ≈ 50% ^{32}Si, with beam contaminants of ^{35}P and ^{40}Ar. These three nuclei were identified at the experimental station by time-of-flight from the end of the A1200. The ^{40}Ar data were also analyzed to determine the $E(2_1^+)$ and B(E2) values as a confirmation of the method. The momentum spread of the accepted fragments was limited to ±0.5% through the use of slits at the first dispersive image of the A1200. The ^{34}Si fragments were produced using the same primary beam/target/wedge combination, but with a different momentum acceptance defined by the A1200 dipole magnets.

The ^{36,38}Si nuclei were produced by fragmentation of a beam of 70 MeV/A ^{48}Ca on a target of 285 mg/cm^2 ^{9}Be. The production of the ^{48}Ca primary beam has been described separately [8]. A thin 5 mg/cm^2 plastic wedge was used to reduce the number of light fragments reaching the experimental end station. This use of a very thin wedge resulted in a large number of different fragments reaching the γ-ray detection area; the fragments were identified by energy loss in a thin fast-plastic detector and by time-of-flight from the end of the A1200. This allowed the study of a large number of different nuclei in the same experiment. The momentum spread of the accepted fragments for this experiment was limited to ±1.5% through the use of slits at the first dispersive image of the A1200. This large acceptance was chosen in order to maximize the number of accepted fragments, while still restricting the momenta enough to allow for separation of the fragments in ΔE/time-of-flight.

The study of nuclear behavior by Coulomb excitation using low-energy beams is well-understood, and requires no elaboration here [9]. The extension of the method to medium-energy (30 – 60 MeV/A) beams, however, places several new constraints on the measurement process. In order to insure that the excitation is exclusively Coulomb-induced, the accepted events must be restricted to forward-scattering such that the minimum impact parameter is at least 5 fm larger than the sum of the radii of the projectile and target nuclei. The scattering angle in the experiments discussed here was restricted to $\theta_{lab} \leq 3.8^o$, which corresponds to minimum impact parameters of 16 – 22 fm. The scattered beam particles were

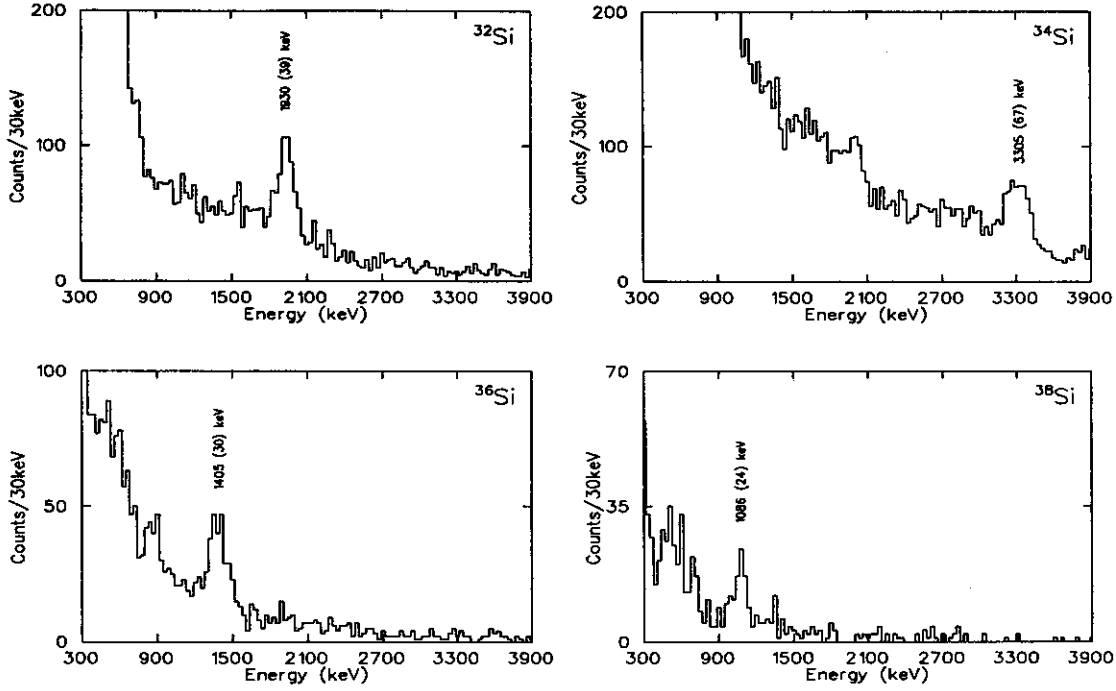

Figure 1: γ-ray spectra in coincidence with detected ^{32,34,36,38}Si ions.

identified in a phoswich detector, in order to exclude events involving violent reactions.

Due to the low production rates of the radioactive nuclei studied, an array of 39 NaI(Tl) detectors was used for γ-ray detection, enclosed in 16.5 cm thick lead shielding. The NaI(Tl) crystals were 19 cm long (5.8 cm diameter), with one phototube on each end so that the position of the incident γ rays could be determined (to $\approx$ 1 cm) by light division. This allows Doppler correction of the γ rays on an event-by-event basis. For further details, the reader is referred to [10].

The background-subtracted γ-ray spectra obtained for ^{32,34,36,38}Si are shown in Figure 1. Doppler-corrections to the energy of the projectile γ ray have been applied on an event-by-event basis. The 547 keV $7/2^+ \rightarrow 3/2^+$ γ-ray peak from the excitation of the ^{197}Au target nuclei appears as an artificially broadened peak in all the spectra. The spectra shown are sums of γ rays detected in 8 of the 11 NaI crystals which comprise the inner ring of the array.

The centroids of the Doppler-shift-corrected γ-ray peaks are shown in Figure 2 and listed in Table 1. It should be stressed that this is the first reported observation of an excited state in ^{36}Si or ^{38}Si. The measured $2^+ \rightarrow 0^+$ γ-ray energies for ^{32,34}Si and ^{40}Ar show good agreement with the known energies (see Table 1). The largest contribution to the uncertainty in γ-ray energy is due to the uncertainty in the γ-ray position in the NaI crystal. The position-calibration of the detectors was performed prior to their placement in the array. It is therefore possible that the actual position of the detector was offset from its assumed position by as much as 4 mm. The contribution to the uncertainty due to such an offset has been included in the errors in Figure 2. The contributions from uncertainties in the beam velocity and energy calibration have also been included in these errors.

The extraction of the B(E2) values was performed following the method of Winther and Alder [11]. The excitation is calculated in first-order perturbation theory. Since no decays from higher-lying states are seen in any of the cases studied herein, this method is expected to be accurate. The extracted

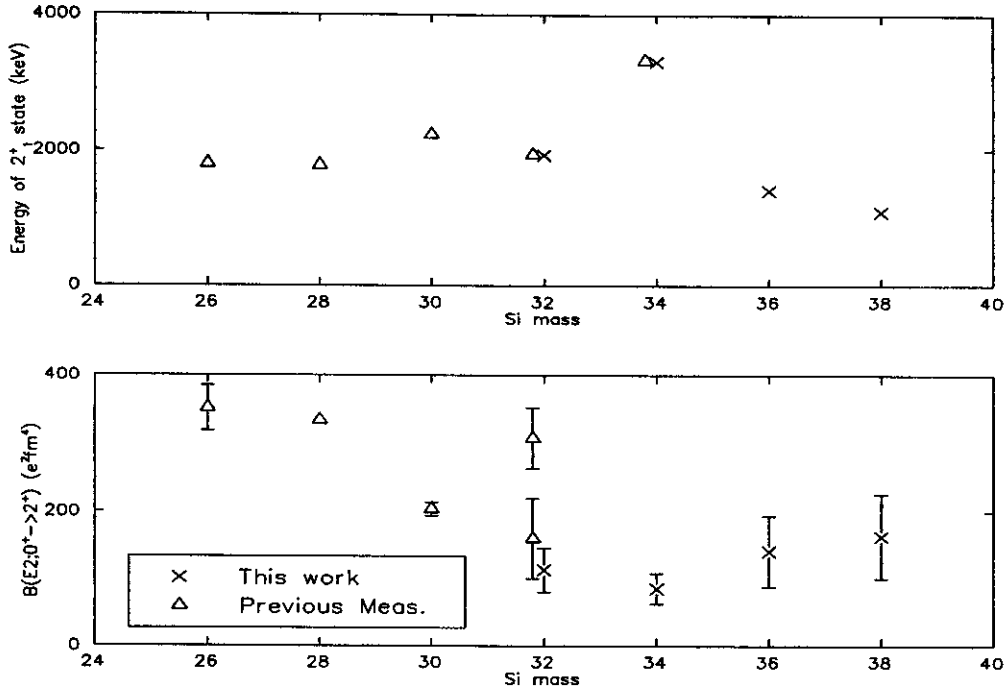

Figure 2: The extracted values of $E(2^+)$ and $B(E2;0^+ \rightarrow 2^+)$ from the present work. The two values shown for ^{32}Si are from references [6] and [7]. Previous measurements for ^{26,28,30}Si have been included to show the trend.

$B(E2;0^+ \rightarrow 2^+)$ values are shown in Figure 2 and listed in Table 1. The two largest contributions to the quoted uncertainties are the statistical uncertainties (in peak size and in background fit) and uncertainties in the efficiency. Below 2.614 MeV the efficiency of the array was measured with calibrated γ-ray sources. For the case of ^{34}Si, the efficiency was determined by extrapolation of the fit. Geant calculations have been performed to test the accuracy of this extrapolation. Using the relative efficiencies from Geant in conjunction with the last measured point results in an efficiency of 1.92 ± 0.27 % at 3.328 MeV, in good agreement with the extrapolation of the fit (1.96 ± 0.27 %). Contributions from the uncertainties in the target thickness, normalization to particle-singles events, angular straggling, angular coverage of the particle detector and beam velocity have also been included.

The extracted B(E2) value for ^{40}Ar shown in Table 1 agrees with the known value of 380 ± 14 e^2fm^4, showing that the use of perturbation theory is valid in these cases. The previously determined values for the B(E2) in ^{32}Si are 160 ± 60 e^2fm^4 [6] and 308 ± 45 e^2fm^4 [7]. The value determined in the present work agrees with the former measurement, but not the latter. The ^{34}Si B(E2) value clearly corresponds to a small degree of collectivity; the present measurement corresponds to 2.6 W.U, which shows that the N=20 shell closure persists to Z=14, and breaks down quite rapidly at Z=12.

a. Present Address: Ludwig Maximilians Universität München, D-85748 Garching, Germany.
b. Department of Physics, Florida State University, Tallahassee, Florida, 32306, USA

Nucleus	$E(2^+)$	prev. meas.	$B(E2;0^+ \rightarrow 2^+)$
^{32}Si	1930 (31)	1941.5 (2)	113 (33)
^{34}Si	3305 (55)	3327.7 (5)	85 (23)
^{36}Si	1405 (26)		141 (53)
^{38}Si	1086 (21)		163 (63)
^{40}Ar	1465 (24)	1460.589 (5)	372 (68)

Table 1: Energies of the first-excited state and B(E2) values leading to this state as determined in the present work.

References

1. P. Baumann et al., *Phys. Lett.* **228B**, 458 (1989).
2. N. Fukunishi, T. Otsuka and T. Sebe, *Phys. Lett.* **296B**, 279 (1992).
3. T. Motobayashi et al., *Phys. Lett.* **B346** (1995) 9.
4. H. Scheit et al., *Phys. Rev. Lett.* **77** (1996) 3967.
5. T. Glasmacher et al., *Phys. Lett.* **395B** (1997) 163.
6. J.G. Pronko and R.E. McDonald, *Phys. Rev.* **C6** (1972) 2065.
7. G. Guillaume *et al., Nucl. Phys.* **A227** (1974) 284.
8. R. Harkewicz, *Rev. Sci. Instr.* **67** (1996) 2176.
9. K. Alder and A. Winther, *Coulomb Excitation*, North-Holland Publication Co., 1975.
10. T. Glasmacher et al., NSCL Annual Report (1995) p. 263.
11. A. Winther and K. Alder, *Nucl. Phys.* **A319** (1979) 518.

COULOMB EXCITATION OF NEUTRON-RICH ARGON AND SULFUR ISOTOPES

H. Scheit, T. Glasmacher, B.A. Brown, J.A. Brown, P.D. Cottle[a], P.G. Hansen, R. Harkewicz, M. Hellström[b], R.W. Ibbotson, J.K. Jewell[a], K.W. Kemper[a], D.J. Morrissey, M. Steiner, P. Thirolf[c], and M. Thoennessen

One of the basic properties of nuclei is their level structure and the strength by which these levels are coupled. This information can be related to the shape of a particular nucleus. Nuclei that are spherical and stiff against deformation show large excitation energies and small coupling strengths. The most spherical nuclei are the ones with magic neutron and proton numbers. Nuclei that are deformed or soft against deformation have small excitation energies and larger coupling strengths. One way to measure the energy of a level and the strength through which it is coupled to the ground state is to excite the nucleus through Coulomb excitation. Since the electro magnetic interaction is well understood, nuclear structure properties can easily be inferred.

A region where little was known about the shape of nuclei is the region of the neutron-rich Sulfur and Argon isotopes. This region is of particular interest because it is located between two major shell gaps, the N=20 and N=28 neutron shell gaps. It is desirable to have a full data set so systematic trends can be observed. It was also predicted that the N=28 shell gap vanishes at Z=16 (^{44}S) [1]. The availability of a high intensity ^{48}Ca primary beam makes it possible to produce secondary beams of these neutron-rich isotopes, through projectile fragmentation, with sufficient particle rates to perform Coulomb excitation experiments. We used this technique to populate low-lying states in ^{38,40,42}S and ^{44,46}Ar.

The secondary beams were obtained by fragmentation of ^{48}Ca and ^{40}Ar beams with energies of up to 80 A MeV in a 379 mg/cm^2 ^{9}Be target located at the mid-acceptance target position of the A1200. A new technique was employed in producing the high intensity ^{48}Ca beam [2]. The purities and intensities of the secondary beams are listed in table 1.

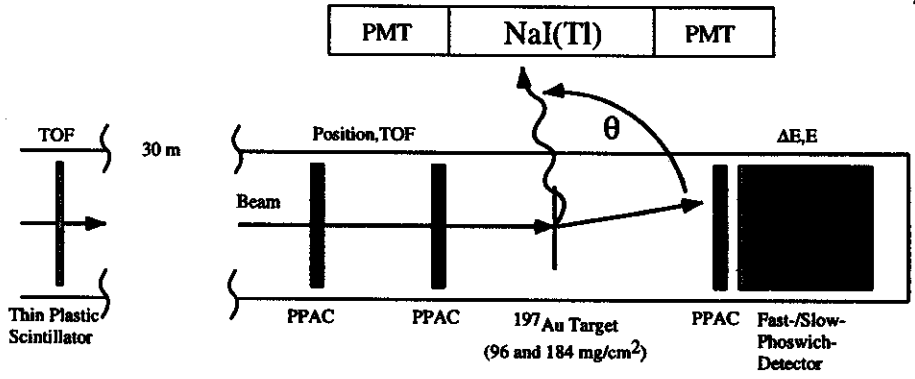

Figure 1: Setup around the secondary target.

We used a ^{197}Au target (93.5 mg/cm^2 for the Argon isotopes and 184.1 mg/cm^2 for the sulfur isotopes)to Coulomb excite the projectile nucleus. After excitation the nucleus decays back to the ground state and emits a gamma ray. These deexcitation gamma rays were detected in an array of 42 position sensitive Na(Tl) detectors. The detectors were cylindrical, about 18 cm long, and 5.75 cm in diameter and oriented parallel to the beam direction as shown in Fig. 1. We used standard photon sources (^{22}Na,^{88}Y,^{152}Eu,^{228}Th) for a position dependent energy and efficiency calibration. A typical energy

resolution is 8% at 662 keV. Because of the large velocity of the beam particles, about 0.3 c, the gamma ray detectors had to be position sensitive in beam direction in order to correct for the Doppler shift. The position resolution was about 2 cm which resulted in an angular resolution of better than 10° for the emitted photon.

Each beam particle was identified before and after the secondary Au target. Before the target, a time of flight measurement between a thin plastic scintilator after the A1200 focal plane and a PPAC located in front of the secondary target provided the particle identification. After the target, an energy loss – total energy measurement in a fast–slow phoswhich detector located at 0° allowed us to reject events from the breakup of the projectile. This 0° detector also allowed us to detect gamma rays in coincidence with particles, therefore reducing the background drastically. In addition it limited the scattering angle of detected particles to less than 4.1 ° in the laboratory and therefore ensured the dominance of Coulomb interaction in the excitation process. The efficiency of the NaI(Tl) array, the measured gamma ray yield in the photo peak, and the total number of beam particles as counted by the 0° detector allowed us to determine the Coulomb excitation cross section. The cross section can then be used to calculate the B(E2,$0^+ \rightarrow 2_1^+$) value which in turn gives a measure of the deformation or collectivity of the nucleus.

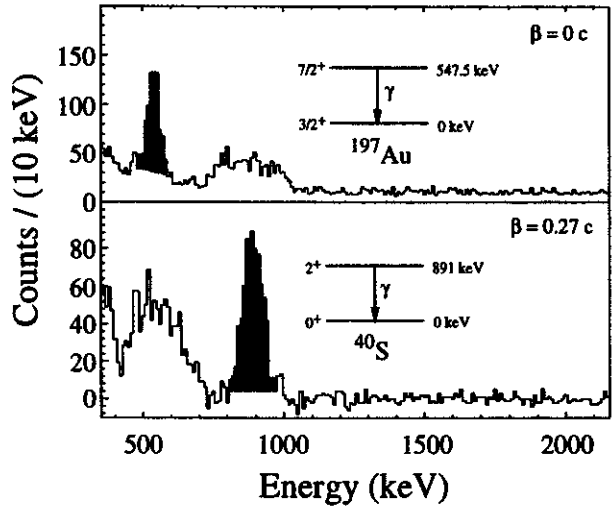

Figure 2: This figure shows a typical gamma spectrum. The top pannel shows the spectrum in the laboratory frame. One can see a sharp peak corresponding to excitation of the target nucleus. After the correction for the Doppler shift (bottom panel) one can see a sharp peak corresponding to the excitation of the projectile.

For all five isotopes we were able to determine the energy of the first excited states, where the known energy of ^{38}S served as a check of the energy calibration, and the B(E2,$0^+ \rightarrow 2_1^+$) values. The measured results are shown in Table 1 and one representative photon spectrum in shown in Figure 2. The results show that ^{40,42}S are deformed whereas the N=28 shell gap persists in ^{46}Ar. A more detailed physics discussion including a comparison to shell model and relativistic mean field calculations can be found in [3].

a. Department of Physics, Florida State University, Tallahassee
b. Gesellschaft für Schwerionenforschung, D-64291 Darmstadt, Germany
c. Current address: Ludwig Maximilians Universität München, D-85748 Garching, Germany

Table 1: Experimental parameters and results. The purity of the secondary beam is for reference only; the secondary fragments were positively identified on an event by event basis and only desired fragments were analyzed. The energy spread of the secondary beam was ±3%.

secondary beam	^{38}S	^{40}S	^{42}S	^{44}Ar	^{46}Ar
Energy (MeV/nucleon)	39.2	39.5	40.6	33.5	35.2
Beam purity	0.99	0.65	0.55	0.99	0.99
typical intensity on target (s^{-1})	50,000	17,000	1,800	50,000	27,000
Energy loss in target (MeV/nucleon)	9.1	8.4	7.9	5.1	4.9
Energy of first excited state (keV)	1286(19)	891(13)	890(15)	1144(17)	1554(26)
$\sigma(\mathrm{E2}; 0^+_{g.s.} \rightarrow 2^+_1, \theta_{\mathrm{lab}} \leq 4.1°)$(mbarn)	59(7)	94(9)	128(19)	81(9)	53(10)
$\mathrm{B(E2}; 0^+_{g.s.} \rightarrow 2^+_1)$ ($\mathrm{e^2fm^4}$)	235(30)	334(36)	397(63)	345(41)	196(39)
$\lvert\beta_2\rvert$	0.246(16)	0.284(16)	0.300(24)	0.241(14)	0.176(17)

References

1. T.R. Werner *et al.*, Phys. Lett. B 335, 259 (1994); Nucl. Phys. A 597, 327 (1996).
2. R. Harkewicz, Rev. Sci. Instr. 67, 2176-2178 (1996).
3. H. Scheit *et al.*, Phys. Rev. Lett. 77, 3967 (1996).

DETERMINATION OF M_N/M_P FOR 2_1^+ STATES IN SINGLE CLOSED SHELL NUCLEI ^{18}NE AND ^{20}O WITH INELASTIC PROTON SCATTERING IN INVERSE KINEMATICS

J.K. Jewell[a], L.A. Riley[a], P.D. Cottle[a], K.W. Kemper[a], M. Chromik, T. Glasmacher, R.W. Ibbotson, D.J. Morrissey, H. Scheit Y. Blumenfeld[b], S.E. Hirzebruch[b], T. Suomijärvi[b], and F. Maréchal[b]

When 2_1^+ states in even-even nuclei are discussed as collective excitations, they are usually assumed to be isoscalar. However, it has been shown [1, 2] that differences can occur between the amplitudes of the motions of the protons and neutrons in these states, especially in semi-magic nuclei. In a particular nucleus, the difference between proton and neutron oscillations can be determined by comparing $B(E2; 0_{gs}^+ \rightarrow 2_1^+)$ reduced matrix elements from two different experimental probes. Madsen, Brown and Anderson [3] pointed out that the comparison of results from low energy (10-50 MeV) proton scattering and electromagnetic measurements is a particularly good method for comparing proton and neutron multipole matrix elements (M_p and M_n, respectively). Until recently, comparisons of M_p and M_n have not been possible in short-lived nuclei. However, recent developments in the production of radioactive beams and techniques for measuring direct reactions in inverse kinematics have made such comparisons possible for the first time.

We measured $B(E2; 0_{gs}^+ \rightarrow 2_1^+)$ reduced matrix elements from low energy proton scattering for the N=8 isotope ^{18}Ne and the Z=8 nucleus ^{20}O in inverse kinematics using 30 MeV/u beams of these radioactive isotopes. Both beams were produced in the A1200 spectrograph [4] and more than 10,000 particles/sec were delivered to the 3.6 mg/cm^2 polypropylene target in each experiment. Scattered protons were detected with the FSU/MSU array of charged particle telescopes.

The angular distributions for the scattered protons (both elastic and inelastic) are shown in Figure 1. The differential cross sections for elastic scattering measured in each telescope were normalized to cross sections calculated using optical model parameters extracted from the ^{20}Ne(p,p) reaction at 30 MeV [5]. RMS deformation parameters β_2 were then deduced from fits using coupled channels calculations with the computer code CHUCK [6]. These results were then combined with electromagnetic $B(E2; 0_{gs}+ \rightarrow 2_1^+)$ data [7] to obtain M_n/M_p results, which are compared with M_n/M_p values for 2_1^+ states of even-even nuclei in the $12 \leq A \leq 26$ mass region in figure 2.

In an isoscalar state, the ratio M_n/M_p is equal to N/Z, the ratio of the neutron and proton numbers. However, 2_1^+ states of semi-magic nuclei often have an isovector contribution [1, 2]. In nuclei with closed neutron shells and open proton shells, M_n/M_p is often less than N/Z. On the other hand, closed proton shell nuclei with open neutron shells often have M_n/M_p¿ N/Z. This can be seen in Figure 2, where N/Z values are illustrated with horizontal lines (both dashed and solid). The nuclei without closed shells (^{12}C, ^{20}Ne, ^{22}Ne, ^{24}Mg and ^{26}Mg) and the doubly-magic nucleus ^{16}O fall close to or on the N/Z lines, while the singly-closed shell nuclei ^{14}C and ^{18}O deviate significantly from N/Z.

The M_n/M_p value for ^{20}O is much larger than N/Z, as is expected for a nucleus with a closed proton shell and an open neutron shell. It might be expected that M_n/M_p would be larger in ^{20}O than in ^{18}O because it is closer to the neutron drip line nucleus ^{24}O, but this trend is not supported by the data.

In contrast, the M_n/M_p result for ^{18}Ne is surprising. While the mirror nucleus ^{18}O shows an isovector contribution clearly, the ^{18}Ne result is consistent with isoscalar nature. In fact, we would expect that M_n/M_p in ^{18}Ne is equal to the reciprocal of the ^{18}O result if isospin symmetry holds, and the data

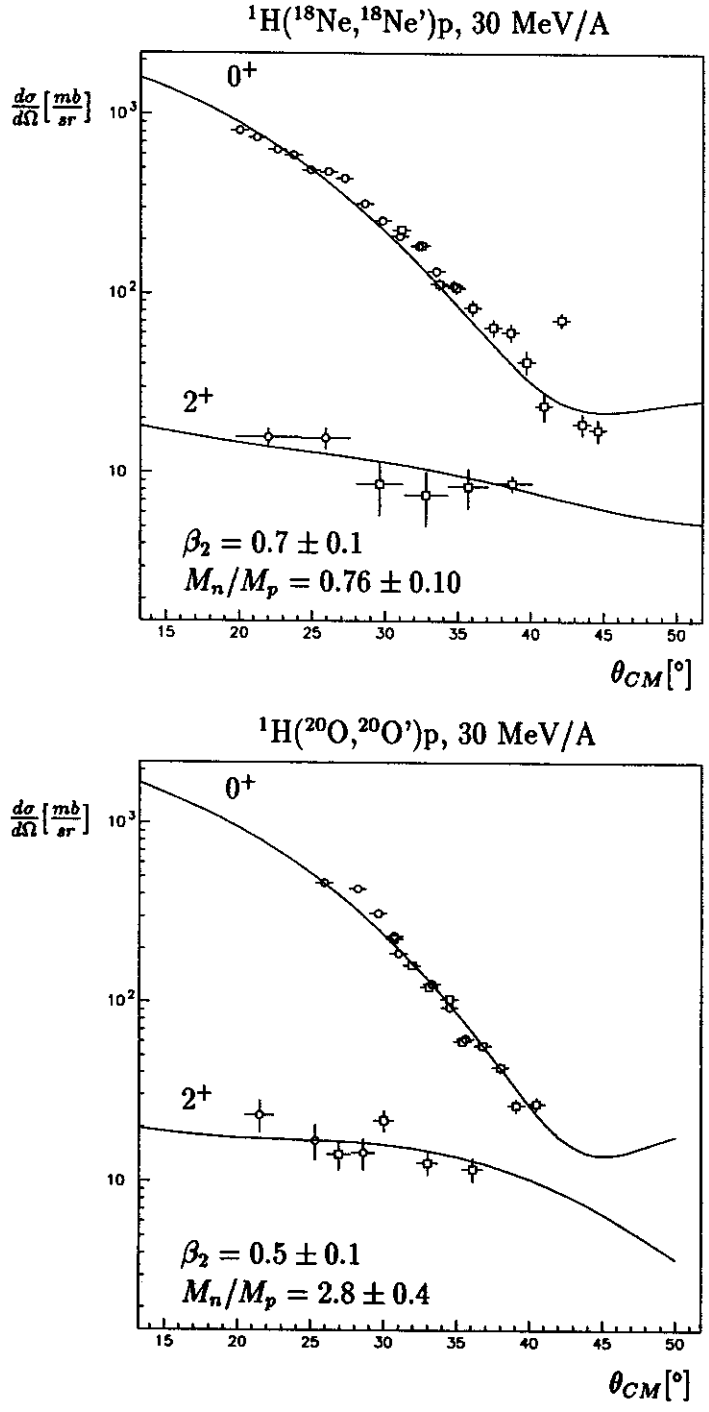

Figure 1: Angular distributions of protons scattered from the ground states and 2_1^+ states of ^{18}Ne and ^{20}O. The smooth curves are coupled channel calculations using known optical model parameters from ^{20}Ne [5] and the RMS quadrupole deformations β_2 giving the best fit to the inelastic cross sections. The corresponding M_n/M_p values are included.

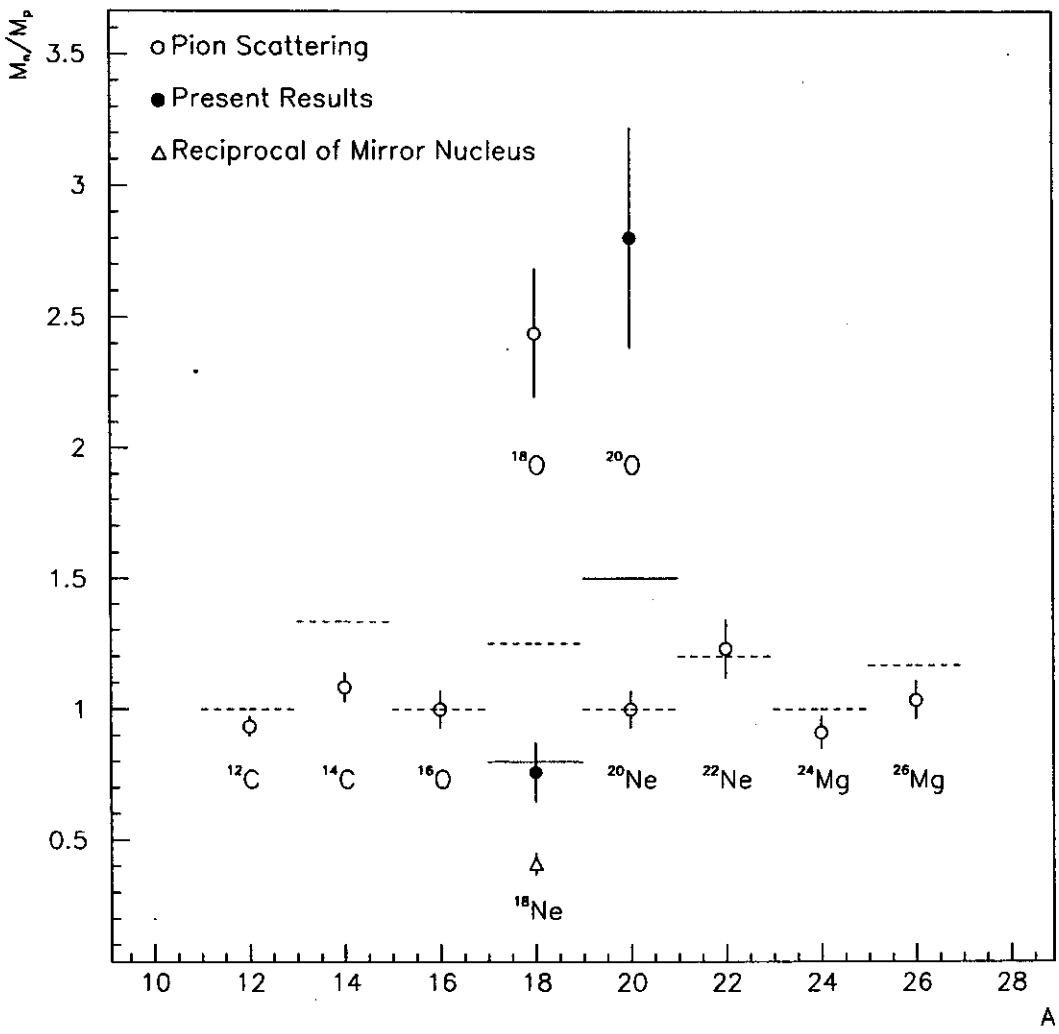

Figure 2: The ratio of neutron to proton multipole matrix elements M_n/M_p of the 2_1^+ states for nuclei in the 12 $\leq$ A $\leq$ 26 mass region. With the exception of those from the present work, the results are from pion scattering data.[8] The dashed lines correspond to the ratio of neutron to proton number N/Z for the pion scattering results and the solid lines to N/Z for the present results.

clearly contrdict this expectation. One possible interpretation of the ^{18}Ne result is that the N=8 shell gap which is so clearly present in ^{14}C and ^{16}O does not occur in ^{18}Ne.

a. Florida State University
b. IPN-Orsay

References

1. A.M. Bernstein, V.R. Brown and V.A. Madsen, Comments Nucl. Part. Phys. 11, 203 (1983).
2. M.A. Kennedy, P.D. Cottle and K.W. Kemper, Phys. Rev. C 46, 1811 (1992).
3. V.A. Madsen, V.R. Brown and J.D. Anderson, Phys. Rev. C 12, 1205 (1975).
4. B.M. Sherrill, *et al.*, Nucl. Inst. and Meth. B70, 298 (1992).
5. R. de Swiniarski, *et al.*, Can. J. Phys. 52, 2422 (1974).
6. P.D. Kunz, University of Colorado report (unpublished).
7. D.R. Tilley, *et al.*, Nucl.Phys. A595, 1 (1995).
8. R.J. Peterson, Phys. Rev. C48, 1128 (1993).

ELASTIC AND INELASTIC SCATTERING OF PROTONS ON ^{38}S IN INVERSE KINEMATICS

T. Suomijärvi[a], J. H. Kelley[a], S. E. Hirzebruch[a], T. Glasmacher, A. Azhari, D. Bazin, Y. Blumenfeld[a], J. A. Brown, P. D. Cottle[b], S. Danczyk, M. Fauerbach, J. K. Jewell[b], K. W. Kemper[b], F. Maréchal[a], D. J. Morrissey, S. Ottini[c], J. A. Scarpaci[a] and P. Thirolf

Direct reactions induced by light particles can provide a wealth of information on nuclear structure and interaction potentials. Since the availability of radioactive beams such studies can be extended to unstable nuclei. In this case the reactions are performed in inverse kinematics and a powerful experimental method is to reconstruct the reaction kinematics by measuring the energy and angle of the recoiling light particle. To perform such experiments, we have developed at the NSCL a silicon-strip array. The first experiment with this array was devoted to the study of elastic and inelastic scattering of protons on the neutron rich ^{38}S isotope.

The silicon-strip array consists of 5 telescopes (recently upgraded to 8) of 5×5 cm active area. Each telescope comprises a 300 μm silicon strip-detector with 16 vertical strips 3 mm wide backed by a 300 μm or 500 μm thick silicon PIN-diode and a 1 cm thick CsI stopping detector read out by 4 photodiodes. Such detectors allow us to measure protons from about 1 MeV up to 50 MeV. The particle identification in the recoil telescopes is performed either by a time-of-flight measurement for particles stopped in the strip-detector or by a ΔE-E measurement for particles stopped in the Si PIN-diode or the CsI-detector. A ΔE-E plastic detector is placed at zero degrees behind the target in order to select the reaction channel of interest and to give a start for the time-of-flight measurement.

The aim of the first experiment performed with the array was to measure elastic and inelastic proton scattering on ^{38}S. The telescopes were placed at 29 cm from the target centered at Θ_{lab}=75° (telescopes 1, 2, 3) and Θ_{lab}=70° (telescopes 4, 5) covering a total angular range of 9.8°. This detector setup allowed us to measure an excitation energy spectrum up to about 5 MeV and an angular distribution between $\Theta_{C.M.}$ = 20° and $\Theta_{C.M.}$ = 45°. An additional run with telescopes 4 and 5 at 67° was performed in order to measure the elastic angular distribution up to larger C.M. angles.

The 39 MeV/nucleon ^{38}S beam was produced by fragmentation of a 85 MeV/nucleon ^{40}Ar beam, provided by the K1200 cyclotron, in a 376 mg/cm^2 ^{9}Be production target. The produced fragments were identified by using the A1200 fragment separator. The beam was purified with a 292 mg/cm^2 aluminium wedge placed in the second dispersive image of the A1200. The intensity of the beam was 3×10^5 particles per second, and the purity was higher than 99%. The angular emittance of the secondary beam was reduced by using collimators, and the momentum spread was limited to Δp/p = 1%. This reduced the beam intensity to about 20 000 particles per second but avoided the use of tracking detectors. The ^{38}S projectiles were scattered on a very thin 2 mg/cm^2 CH_2 target in order to limit the energy loss and angular straggling of recoiling low energy protons.

Figure 1 displays a scatterplot of laboratory energy vs. angle for recoiling protons from the ^{38}S scattering. Elastic scattering and inelastic scattering to the first 2$^+$ state of ^{38}S, known to be located at 1.29 MeV, are clearly separated. The insert shows the excitation energy spectrum for an angular bin between 27° and 30° in the CM frame. The overall angular resolutions were on the order of 1.6° FWHM in the laboratory frame and 3.2° FWHM in the CM frame. The primary source of angular uncertainty came from the angular acceptance introduced by the 3 mm strip size and the ~4 mm FWHM beam spot

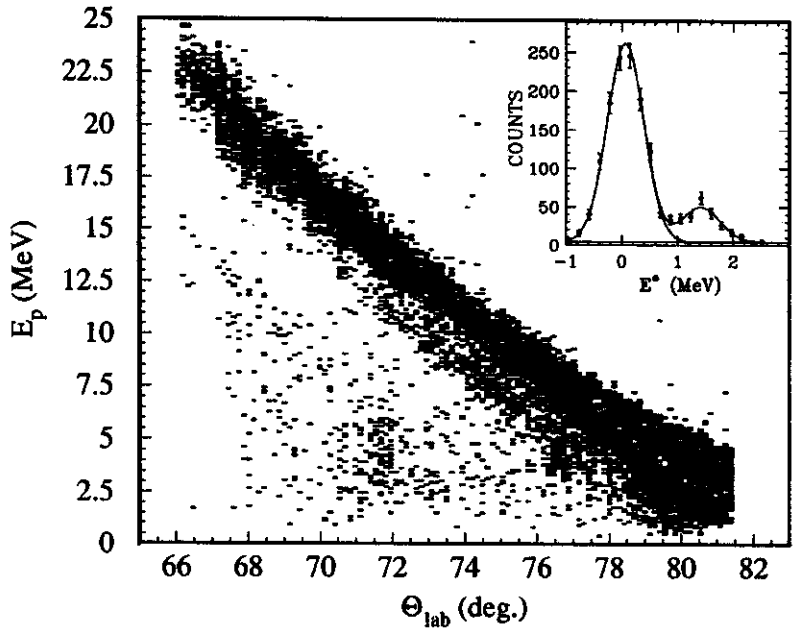

Figure 1: Energy vs. angle scatterplot for recoiling protons.

size. The excitation energy resolution, which depends largely on the laboratory angular resolution, varies from around 600 keV at low CM angles to 900 keV at higher CM angles. The background is very low, suppressed by requiring that a heavy ejectile be observed in the 0° ΔE-E detector in coincidence with scattered protons.

The elastic scattering and 2^+ angular distributions are shown on fig. 2. Note that no arbitrary normalization is involved here. Coupled-channels predictions using the Becchetti-Greenlees parameterization [1] are shown (dotted line) in comparison with the data. A second calculation, shown as the solid line in figure 2, uses optical model parameters for ^{40}Ar(p,p) [2] and gives slightly better agreement with the measured ground state distribution, in particular at small angles. The β_2 value is extracted by normalizing the coupled channel calculation to the 2^+ state cross section. The value obtained is β_2=0.35±0.04 and does not depend on the optical potential used.

Particularly interesting information on the isoscalar or isovector character of the 2^+ oscillation is given by the ratio of the neutron and proton multipole matrix elements M_n/M_p3. This ratio can be obtained by combining the β_2 values measured by electromagnetic and nuclear excitations using the formula derived in ref.4. The electromagnetic β_2 for the 2^+ state of ^{38}S was measured in a Coulomb excitation experiment at the NSCL and yielded β_2=0.25±0.025. This yields M_n/M_p = 2.0±0.4 for the 2_1^+ state in ^{38}S, and thus M_n/M_p = (1.5±0.3)N/Z, which is incompatible with the value of N/Z expected for a pure isoscalar collective excitation. The large M_n/M_p value for ^{38}S can be qualitatively understood by considering the ^{38}S nucleus as a ^{36}S core plus two valence neutrons forming a neutron skin. In this case, the two neutrons drive the oscillation and the core polarization is not sufficient to restore the isoscalar character of the excitation. It would now be interesting to investigate the persistence of such a structure for larger neutron numbers, for which the neutron skin effects may be more pronounced. In this aim, a similar experiment has recently been performed for ^{40}S at the NSCL.

a. Institut de Physique Nucléaire, IN_2P_3-CNRS, 91406 Orsay, France

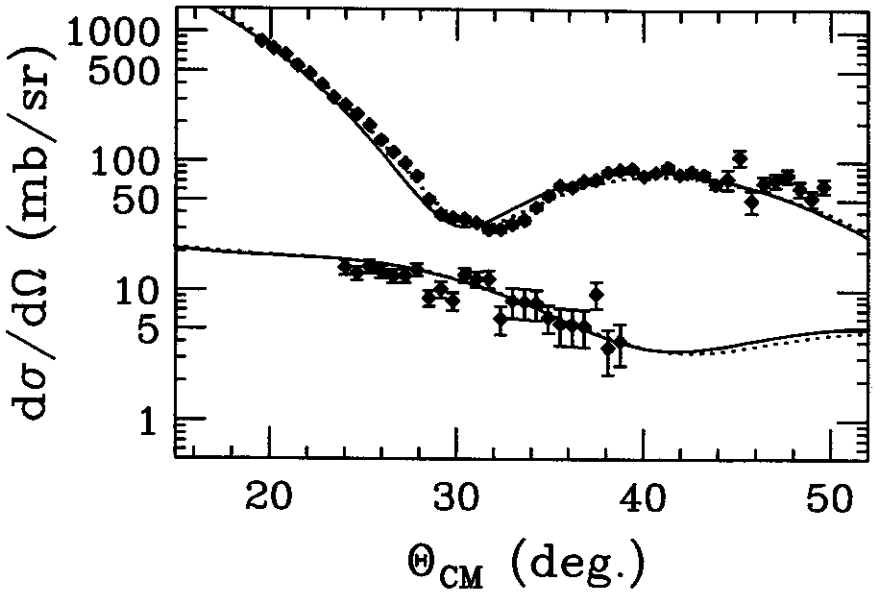

Figure 2: Elastic scattering and 2^+ angular distributions. Solid and dotted lines correspond to coupled-channel calculations, see text.

b. Department of Physics, Florida State University, Tallahassee, FL 32306
c. SEPhN, DAPNIA, CEA Saclay, 91191 Gif sur Yvette, France

References

1. F. D. Bechetti, Jr, and G. W. Greenlees, Phys. Rev. 182 (1969) 1190.
2. E. Fabrici et al., Phys. Rev. C 21 (1980) 830.
3. M. A. Kennedy et al., Phys. Rev. C 46 (1992) 1811.
4. A. M. Bernstein et al., Comments Nucl. Part. Phys. 11 (1983) 203.
5. H. Scheit et al., Phys. Rev. Lett. 77 (1996) 3967.

OBSERVATION OF THE GAMMA DECAY OF THE FIRST EXCITED STATE OF ^{17}Ne

M. J. Chromik[a], B. A. Brown, M. Fauerbach, T. Glasmacher, R. Ibbotson,
H. Scheit, P. G. Thirolf[a], and M. Thoennessen

The search for the di-proton (^{2}He) decay is one of the exciting topics of nuclear physics at the proton-dripline. In lighter nuclei ^{17}Ne is the most promising candidate, because the first excited state in ^{17}Ne is bound with respect to one proton emission but unbound with respect to two-proton emission. This possible di-proton branch would be in direct competition with the γ-decay to the ground state in ^{17}Ne. So far none of these decay modes has been observed. Since lifetime estimates are favouring the γ branch, the search for the γ-decay of the first excited state in ^{17}Ne was our first approach to this nuclei [1].

The sequential decay from the first excited state in ^{17}Ne will be suppressed, since the first low lying states of ^{16}F are located above the first excited state in ^{17}Ne and are quite narrow. Thus the only two remaining possible decay-modes are the two-proton decay to the ground state in ^{15}O or the γ-decay back to the ground state in ^{17}Ne.

A 100 MeV/nucleon ^{20}Ne beam was extracted from the K1200 cyclotron and bombarded a ^{9}Be target. The fragments were then mass analysed with the A1200 fragment separator and the beam of interest (^{17}Ne with 60 MeV/nucleon) was sent to the experimental area. The first excited state in ^{17}Ne was populated via intermediate energy Coulomb excitation. Our experimental setup had to fullfill the following requirements: The projectile had to be Coulomb-excited and the projectile-like reaction products had to be identified after the target in coincidence with the deexcitation γ-rays. Moreover, in order to allow for the Doppler correction ($\beta \approx 0.3$) the measurement of the emission angle θ as shown in Figure 2 was required. The latter implies the measurement of the trajectory of the projectile and the angle into which the γ-ray is emitted. The ΔE,E Fast-Slow-phoswich detector and TOF measurements provided the particle identification. The trajectory of the projectile was measured with PPACs in front of and behind the target. The energy of the emitted γ-rays and their emission angles were measured with the NaI-detectors. In order to get a sufficient position-resolution a phototube was connected to each end of the NaI-crystals. The position of the incident photon could be determined with an accuracy of $\approx$ 2cm, which corresponds to an accuracy for θ of $\approx 10°$. 38 of these detectors were placed in concentric rings around the beam axis. The experimental setup is shown in Figure 2 and described in more details in Ref. [1,2].

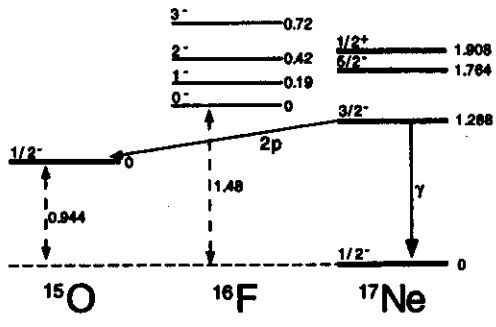

Figure 1: Level scheme of the low lying states in ^{15}O, ^{16}F and ^{17}Ne.

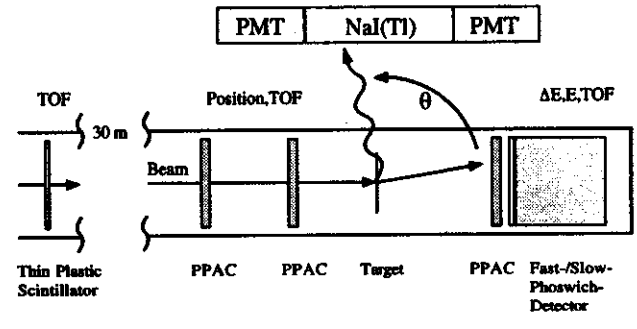

Figure 2: Experimental setup used for the intermediate energy Coulomb excitation experiment.

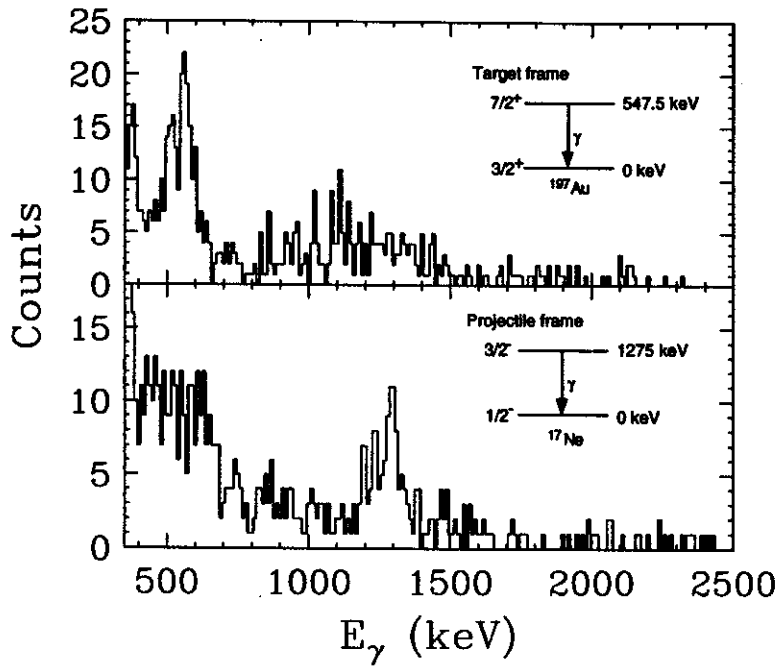

Figure 3: The measured γ-decay spectra. In the projectile rest frame (top) the 7/2- to 3/2- transition in the ^{197}Au target appears. In the projectile rest frame this peak broadens, but at 1275(22)keV a sharp peak from the projectile appears, while the peak corresponding to the transition in ^{197}Au broadens.

The measured decay spectra for both the target rest frame and the projectile rest frame are shown in Figure 3. We observed the γ-decay from the first excited state of ^{17}Ne to the ground state at an energy of 1275(22)keV. In order to obtain an estimate of the branching ratio between the observed γ-decay and a potential two-proton decay, we calculated the excitation cross section using the virtual photon method (see e.g. [3]) and compared the number of expected decays with the number of observed decays. The measured γ-branch accounts only for $\approx$ 43 % of the total excitation cross section, which could be an evidence for the existence of a two-proton decay branch. However, this would be in disagreemeent with the calculated lifetimes which strongly favour the γ-decay. Motivated by these findings a dedicated experiment was performed to search for the 2p-branch, which is described in [4].

a. Present address: Ludwig Maximillian Universität, 85748 Garching, Germany.

References

1. M. J. Chromik, B. A. Brown, M. Fauerbach, T. Glasmacher, R. Ibbotson, H. Scheit, P. Thirolf, and M. Thoennessen, Phys. Rev. C 55, 1676 (1997).
2. H. Scheit, T. Glasmacher, B. A. Brown, J. A. Brown, P. D. Cottle, P. G. Hansen, R. Harkewicz, M. Hellström, R. Ibbotson, J. K. Jewell, K. W. Kemper, D. J. Morrissey, M. Steiner, P. Thirolf, and M. Thoennessen, Phys. Rev. Lett. 77, 3967 (1996).
3. C. A. Bertulani and G. Baur, Phys. Rep. 163, 299 (1988).
4. P. G. Thirolf, A. Azhari, M. J. Chromik, T. Glasmacher, R. Ibbotson, R. A. Kryger, H. Scheit, M. Thoennessen, P. J. Woods, and S. Yokoyama, NSCL, Annual Report 1996, (1997).

TEMPERATURE DEPENDENCE OF THE GIANT DIPOLE RESONANCE IN EXCITED ^{120}Sn AND ^{208}Pb NUCLEI

T. Baumann[a], E. Ramakrishnan[b], and M. Thoennessen

The study of the influence of temperature and angular momentum on properties of the giant dipole resonance (GDR) in excited nuclei is of high current interest [1]. A broadening of the GDR width with excitation energy was observed in heavy-ion fusion evaporation measurements performed on excited Sn isotopes [2,3]. In heavy ion fusion measurements the excited nuclei are populated in high angular momentum states and therefore it is difficult to investigate the temperature-related evolution of the resonance decoupled from angular momentum effects.

Recent measurements employing light-ion inelastic scattering have demonstrated the feasibility of studying the GDR built on highly excited states of nuclei [4]. In light-ion inelastic scattering, the angular momentum transferred to the target nuclei is very low and it is thus possible to decouple the effect of temperature from angular momentum in these measurements. Furthermore, the excitation energy dependence of the GDR can be studied over a large range of energies by gating on the energy loss of the projectile nuclei.

Figure 1 displays the measured GDR width (filled circles) in excited ^{120}Sn and ^{208}Pb nuclei populated by inelastic scattering of 40 and 50 MeV/nucleon α particles, as a function of nuclear temperature [4]. The resonance width was extracted by comparing statistical model calculations to high energy γ-ray spectra measured in coincidence with the inelastically scattered projectile nuclei. The nuclear temperature was obtained from the excitation energy by employing an energy dependent level density parameterization [4,5].

This observed increase of the GDR width with increasing excitation energy has been explained by the adiabatic coupling of the resonance to shape variations of the nucleus induced by temperature and angular momentum [1], and by a convolution of Landau damping (one-body) with the damping due to two-body collisions [6].

Simple estimates of the adiabatic coupling model predict approximately a $\sqrt{T}$ dependence of the width as a function of temperature [7], whereas the collisional model predicts a T^2 dependence [8], although this is still controversial because recently it was argued that the temperature dependence should be extremely weak [9].

As shown in the top panels of Figure 1, the width increase is consistent with a quadratic dependence on temperature (dashed), which is expected from a two body collisional damping model. In contrast, a $\sqrt{T}$ dependence, corresponding to the adiabatic coupling and shown as the solid line in the two top panels of Figure 1 describes only the ^{120}Sn data reasonably well whereas it fails to describe the observed increase in ^{208}Pb.

However, these are only simple estimates and the full calculations were performed for both models [1,6]. The results of the collisional model are shown as dashed lines in the lower panels of Figure 1. The calculated dependence is weaker than T^2 and although it can reproduce the ^{208}Pb data it fails to reproduce the ^{120}Sn data [6]. The results of the adiabatic coupling model (solid lines in lower panels) are able to reproduce the trend of both data sets reasonable well. They both still show the general $\sqrt{T}$ dependence. The upper solid line in the ^{120}Sn calculation includes the effect of the evaporation widths which increases rapidly with increasing excitation energy, and improves the agreement between the calculation and the

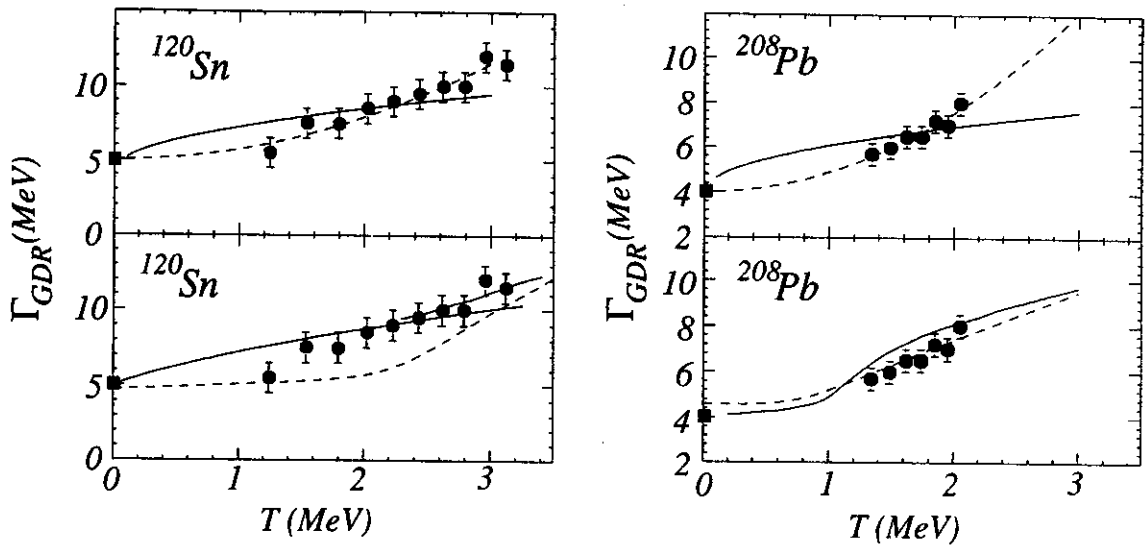

Figure 1: The extracted GDR widths for ^{120}Sn (left) and ^{208}Pb (right) as a function of nuclear temperature. The ground state value is included at zero temperature. The upper panel includes fits with a $\sqrt{T}$ dependence (solid) and a T^2 dependence (dashed) and the lower panels compare the data with adiabatic coupling calculations (solid) and collisional damping calculations (dashed).

highest temperature data points [1]. The important difference between ^{120}Sn and ^{208}Pb is the strong shell effects present in the latter case, which shift the onset of the $\sqrt{T}$ behavior to approximately 1 MeV, at which the shell effects are washed out.

Direct comparisons of the adiabatic and collisional damping calculations with the data is not straight forward due to the critical dependence of the temperature on the level density parameter. In order to obtain a more quantitative description of the data, it is necessary to incorporate the calculated GDR strength function in the statistical model code and compare the experimental spectra directly and not just the extracted GDR width. These calculations are currently in progress.

a. Gesellschaft für Schwerionenforschung, Darmstadt, Germany.
b. Cyclotron Institute, Texas A&M University, College Station, TX 77843.

References

1. W. E. Ormand *et al.*, Phys. Rev. Lett. 77, 607 (1996); Nucl. Phys. A614, 216 (1997).
2. J. J. Gaardhøje *et al.*, Phys. Rev. Lett. 53, 148 (1984); *ibid.* 56, 1783 (1986).
3. D. R. Chakrabarty *et al.*, Phys. Rev. C 36, 1886 (1987).
4. E. Ramakrishnan *et al.*, Phys. Rev. Lett. 76, 2025 (1996), Phys. Lett. B 383, 252 (1996).
5. T. Baumann *et al.*, Proc. of the XXXI Zakopane School of Physics, to be published in Acta Physica Polonica (1996).
6. V. Baran *et al.*, Nucl. Phys. A599, 29c (1996); M. DiToro, private communication.
7. R. A. Broglia *et al.*, Nucl. Phys. A28, 517 (1992).
8. A. Smerzi *et al.*, Phys. Rev. C 44, 1713 (1991).
9. P. Donato *et al.*, Phys. Lett. B 383, 15 (1996).

LONGITUDINAL MOMENTUM DISTRIBUTIONS AND E2 TRANSITIONS IN THE COULOMB DISSOCIATION OF ^{8}B

B.S. Davids, S.M. Austin, H. Esbensen[a], B.M. Sherrill, D.W. Anthony, D. Bazin, B. Blank[b], J.A. Caggiano, M. Chartier, P. Hui[c], C.F. Powell, H. Scheit, M. Steiner, P. Thirolf[d]

For nearly thirty years there has existed a discrepancy between calculated and measured high energy solar neutrino fluxes. Experiments have consistently measured a smaller flux than standard solar models predict. Most of the measured high energy solar neutrino flux is produced by the β^+ decay of ^{8}B. Hence, the disagreement between the observed and predicted high energy solar neutrino fluxes is known as the ^{8}B solar neutrino problem. Deficits in the fluxes of lower energy solar neutrinos from p+p reactions and the decay of ^{7}Be have also been observed [1]. The solar models require as input the low energy cross section factors of several nuclear reactions. It is common to write nuclear reaction cross sections of astrophysical importance as the product of a modestly energy-dependent cross section factor S(E), which contains all of the strictly nuclear effects, and an exponential factor that contains the Coulomb penetrability. Of all the nuclear reactions believed to occur in the sun, the most important for the ^{8}B solar neutrino problem is also the least well known, the radiative capture reaction ^{7}Be(p,γ)^{8}B.

The latest high precision determination of the low energy cross section factor of the ^{7}Be(p,γ)^{8}B reaction, $S_{17}(0)$, was performed at Argonne [2]. This finding, which had a quoted uncertainty of 12%, is in disagreement with previous work. The principal source of uncertainty in this experiment was the thickness of the radioactive ^{7}Be target.

In 1994, a group at RIKEN reported using a different technique to extract $S_{17}(0)$ [3]. These researchers obtained the cross section for the Coulomb dissociation reaction ^{208}Pb(^{8}B,^{7}Be p)^{208}Pb at 46.5 MeV/u. In such an experiment, the heavy target creates an intense virtual photon field in the rest frame of the incident ^{8}B. The principle of detailed balance yields a relation between the radiative capture cross section and the corresponding photodissociation cross section for photons of a given multipolarity. These authors quote an experimental uncertainty of 19% for this measurement, which is worse than the Argonne measurement. However, in the future, one should expect this uncertainty will be reduced through improvements in apparatus.

A significant controversy arose over the interpretation of the RIKEN data. Although the radiative capture reaction proceeds almost exclusively by electric dipole transitions, E2 photons can contribute significantly in Coulomb dissociation. The analysis published by the RIKEN experimenters assumed that the measured cross section was due entirely to E1 transitions, and that the E2 contribution was negligible. The controversy centered on the role of E2 transitions in the RIKEN experiment. Some theorists maintained that the E2 contribution should not be neglected [4,5,7]. It appears difficult to estimate reliably the E2 strength on theoretical grounds. Theoretical determinations based on the RIKEN data [4,5,6,7] have large uncertainties and may fail to account for nuclear effects properly. If the E2 strength in Coulomb dissociation is appreciable, then the measurement of the RIKEN group would imply that the E1 contribution to the measured cross section is smaller than is currently believed. This would mean that the radiative capture low energy cross section factor is smaller, and therefore that the calculated high energy solar neutrino flux is smaller than is currently believed.

First order perturbation theory calculations of the Coulomb dissociation of ^{8}B [8] predict that the distribution of the longitudinal momenta of emitted ^{7}Be fragments will be asymmetric due to interference between E1 and E2 transition amplitudes. When higher order dynamical effects proportional to the cube of the target charge are considered, the predicted asymmetry is somewhat reduced, but remains observable [8]. Increasing the beam energy is also expected to reduce the

asymmetry because the ratio of the number of virtual E1 photons to E2 photons increases with beam energy

Hence, an effective way to gauge the strength of E2 transitions in this process is to look for the signature of asymmetry in the longitudinal momentum distribution [8]. Such a measurement is a critical test of the idea that the Coulomb dissociation of ^{8}B is accurately described by the dynamical model of reference 8, and that the E2 strength in this reaction can be extracted from the longitudinal momentum distribution.

A study of the longitudinal momentum distributions of ^{7}Be fragments from the breakup of 40 MeV/u ^{8}B on a gold target has been performed at the NSCL [9]. The data from this experiment favor an asymmetric momentum distribution of roughly the predicted size, but the uncertainties due to low statistics prohibit a definitive conclusion.

In 1996, the RIKEN group reported on the results of an experiment designed to determine the E2 contribution to the Coulomb dissociation of ^{8}B by measuring the angular distributions of the emitted fragments [10]. While acknowledging the possibility of large systematic errors, they found that the E2 contribution is much smaller than all published theoretical predictions. They concluded that their original analysis, which considered only E1 transitions, was correct.

It was decided to use the new S800 spectrometer at the NSCL to carry out a high precision, high statistics measurement of the longitudinal momentum distribution of ^{7}Be fragments from the Coulomb dissociation of ^{8}B. In our experiment, 125 and 100 MeV/u ^{12}C beams from the K1200 cyclotron of the National Superconducting Cyclotron Laboratory at Michigan State University bombarded a 1900 mg/cm^2 Be target. A 247 mg/cm^2 Aluminum-equivalent plastic wedge was used with 0.5% momentum acceptance slits to separate 83 and 45 MeV/u ^{8}B beams in the A1200 fragment separator. The angular acceptances were 20 mrad in θ, and 40 mrad in φ. A thin scintillator was placed near the exit of the A1200 for flight time and rate determinations. The secondary beam consisted of ^{9}C, ^{8}B, ^{7}Be, and ^{6}Li. A 300 μm Silicon pin diode detector was placed on a target drive at the S800 target position to periodically monitor the composition of the secondary beam. The ^{8}B nuclei were broken up in Be, Ag, and Pb targets at the S800 target position. The S800 spectrometer was set at 0° to detect the ^{7}Be breakup fragments.

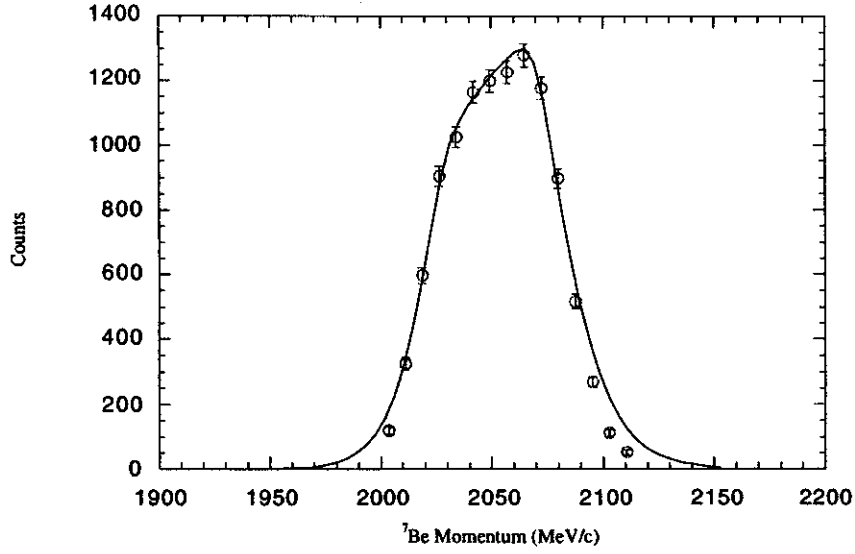

Figure 1: Preliminary longitudinal momentum distribution of ^{7}Be fragments from the Coulomb dissociation of 45 MeV/u ^{8}B on a Pb target. The points are the experimental data. The curve was generated with the dynamical model of Esbensen and Bertsch.

We utilized the standard S800 focal plane setup: 2 position-sensitive cathode readout drift chambers (CRDCs), an ionization chamber, and 3 thick plastic stopping scintillators. Reaction product identification was achieved by comparing the energy losses, times-of-flight, and total energies of the particles. The momenta of the ^{7}Be fragments were measured by their positions in the first CRDC.

The analysis of this experiment is underway. We will extract cross sections and E2 transition strengths for the Coulomb dissociation of ^{8}B on Ag and Pb at two energies. As the figure illustrates, preliminary analysis of the data reveals that this reaction is well described by the dynamical model of Esbensen and Bertsch. The evident asymmetry of the distribution suggests that E2 transitions play a role in the Coulomb dissociation of ^{8}B.

a. Physics Division, Argonne National Laboratory, 9700 S. Cass Ave., Argonne, IL 60439
b. Centre d'Etudes Nucléaires de Bordeaux-Gradignan, F-33175 Gradignan Cedex, France
c. Lincoln Laboratory, Massachusetts Institute of Technology, 244 Wood Street, Lexington, MA 02173
d. Ludwig Maximilians Universität München, Am Coulombwall 1, D-85748 Garching, Germany

References

1. J.N. Bahcall, Ap. J. **467**, 475 (1996).
2. B.W. Filippone, A.J. Elwyn, C.N. Davids, and D.D. Koetke, Phys. Rev. C **28**, 2222 (1983).
3. T. Motobayashi *et al.*, Phys. Rev. Lett. **73**, 2680 (1994).
4. K. Langanke and T.D. Shoppa, Phys. Rev. C **49**, R1771 (1994).
5. K. Langanke and T.D. Shoppa, Phys. Rev. C **51**, 2844 (1995).
6. M. Gai and C.A. Bertulani, Phys. Rev. C **52**, 1706 (1995).
7. K. Langanke and T.D. Shoppa, Phys. Rev. C **52**, 1709 (1995).
8. H. Esbensen and G. Bertsch, Nucl. Phys. A **600**, 37 (1996).
9. J.H. Kelley, *et al.*, Phys. Rev. Lett. **77**, 5020 (1996).
10. T. Kikuchi, *et al.*, submitted to Nucl. Phys. A (1996).

PROBING THE HALO STRUCTURE OF ^{19,17,15}C and ^{14}B

D. Bazin, W. Benenson, J. Brown[a], B. Davids, M. Fauerbach[b], P.G. Hansen, P. Mantica, D.J. Morrissey, C.F. Powell, B.M. Sherrill, and M. Steiner

We have measured the parallel momentum distributions of outcoming fragments in the one-neutron breakup of the odd-mass carbon isotopes ^{19,17,15}C and ^{14}B. Owing to their low neutron separation energy, the study of this series of nuclei is of particular interest regarding the appearance of the halo phenomenon. The breakup of these nuclei was induced by both nuclear and Coulomb excitations using Be and Ta targets, in an attempt to explore the role of the breakup mechanism on the final momentum distributions. The nuclear breakup results are compared to two calculations. One used the Hankel functions, which are the exact solutions for the external wave function of a bound state [9, 1]. The other used Wood-Saxon single particle wave functions weighted by spectroscopic factors obtained from shell-model calculations [5].

1. Introduction

As our knowledge on nuclei far from stability deepens, it becomes more and more apparent that nuclear halos are a rather general feature of loosely bound nuclei. As the binding energy becomes smaller in the vicinity of the drip lines, the valence nucleon(s) can tunnel out of the central potential, and therefore enhance the diffuseness of the nuclear surface. Eventually, this leads to a delocalization of the valence nucleon(s) which can be pictured as a halo surrounding the remaining core of the nucleus. The appearance of this halo is determined by the height of the potential barrier, which itself depends on the binding energy, the angular momentum and, for protons, the Coulomb potential.

2. Experimental program

In order to investigate the formation of halos in nuclei, we present the results of experiments performed on the series of nuclei ^{19,17,15}C and ^{14}B. The choice of these nuclei is motivated by the broad range of binding energies and possibly angular momentum that they display. ^{15}C and ^{14}B have presumably very similar $\ell = 0$ neutron shell structures, confirmed in ^{15}C by ^{14}C(d,p) reaction angular distributions [8]. ^{19}C has been shown to be the heaviest halo nucleus so far [2], but its detailed structure remains uncertain partly because of the large error on its mass. The ^{17}C structure is still unknown experimentally, and shell model calculations predict a very close proximity between the s-orbit and the d- orbit in this nucleus. The known characteristics of these four nuclei are summarized in Table 1. shell model predictions are also included when the experimental orbitals are unknown.

Shell-model calculations using the WBP interaction [23] indicate that the well known inversion of the $0d_{5/2}$ and $1s_{1/2}$ orbits in ^{15}C is reproduced by the calculation, but also that the situation for ^{17}C and ^{19}C is not so clear, and there could be a strong mixing of the two components in the ground state of those two nuclei. Relativistic Mean Field calculations on the carbon isotopes [17] predict a deformation of the neutron-rich isotopes which peaks at ^{18}C, and ground states of $1/2^+$, $3/2^+$ and $1/2^+$ for ^{15}C, ^{17}C and ^{19}C respectively.

3. Experiment

Nucleus	S_n	J^π g.s.	Valence neutron orbit
^{14}B	970 ±21 keV	2^- (exp.)	$1s_{1/2}$ (exp.)
^{15}C	1218.1 ±0.8 keV	$1/2^+$ (exp.)	$1s_{1/2}$ (exp.)
^{17}C	729 ±18 keV	$3/2^+$ (calc.)	$0d_{5/2}$ (calc.)
^{19}C	160 ±110 keV	$1/2^+$ (calc.)	$1s_{1/2}$ (calc.)

Table 1: Characteristics of the studied nuclei. Shell model predictions have been included when the orbitals are unknown experimentally (calc.).

In this experiment the halo structure of the studied nuclei was probed using breakup reactions in which the valence neutron is removed from the projectile, and the momentum of the recoiling core is measured. According to the complementarity principle, the width of the valence neutron distribution in momentum coordinates is inversely proportional to its width in space coordinates, i.e. the spacial extend of the valence neutron wave function. In the plane wave approximation [20], the one-neutron removal cross-section is proportional to the internal momentum distribution of the removed particle. It would therefore provide a direct measurement of the internal wave function via a Fourier transform, as it is done in atomic physics [13] to probe the wave function of valence electrons. Unfortunately, this assumption is not realistic in a nucleus as it does not take into account the nuclear absorption processes which occur because of the short range of the strong interaction. However, these effects have been shown to affect only the transverse component of the momentum distribution [4], whereas the parallel component remains mostly unaltered. This method has been successfully used in many experiments (see for instance [12, 15, 11]), including our previous study of the halo of ^{19}C [2].

The selection of the one-neutron removal channels restricts the total reaction cross-section to impact parameters values that only lead to the destruction of the halo. Reactions leading to the breakup of the core do not contribute to the momentum distributions, which therefore only contain information about the tail of the wave function. This localization or shadowing effect [9] to the outer region of the wave function leads to a modification of the momentum distribution (mostly a suppression of the tails) and a reduction of their width. This effect is taken into account in the calculations by integrating only for impact parameters greater than $b_{min} = R_C + R_T$ where R_C and R_T are the core and target radii respectively.

The experiment was performed on the A1200 [22] fragment separator at the National Superconducting Cyclotron Laboratory. The secondary beams of ^{14}B, ^{15}C and ^{17}C were produced by fragmenting an ^{18}O beam at 100 MeV/u on a 790 mg/cm^2 thick Be target. Because their production cross-section from ^{18}O is smaller, the ^{19}C were produced by fragmenting an ^{40}Ar beam at 100 MeV/u on a 470 mg/cm^2 thick Be target. The separator was operated in dispersion-matched mode [6] in which the reaction target is placed at a dispersive location, and the intrinsic dispersion of the secondary beam is compensated for by the last section of the spectrometer. The magnetic rigidity of this last section is set according to the momentum of the outgoing core fragment.

As fragment separation was provided by the first section of the spectrometer, the selection of the fragments was in magnetic rigidity only, which introduced numerous contaminants in the secondary beams. However, this allowed some of the nuclei of interest to be transmitted simultaneously, such as ^{14}B and ^{17}C which were transmitted at the same Bρ setting. Although other reactions and scattered particles from the contaminants arrived at the focal plane, the group of events corresponding to the one-neutron breakup of the nuclei of interest was uniquely identified because of their unique time of flight

and the specific setting of the magnetic rigidities of the A1200. The elastically scattered $^{A-1}$Z nuclei were not transmitted through the last section of the spectrometer because their momentum did not match the rigidity.

The reaction targets of Be and Ta had thicknesses of 190 mg/cm^2 and 295 mg/cm^2 respectively, chosen for equivalent energy loss. The situation is particularly favorable in the case of a neutron stripping reaction, since the differential energy loss between ^{A}Z and $^{A-1}$Z is very small. The thickness limitation was the energy straggling, chosen to be about the same magnitude as the resolution of the spectrometer. The momentum dispersion and the resolution were measured by stepping the elastically scattered secondary beam across the focal plane. This also allowed the mapping of the acceptance of the last section of the A1200. The momentum resolution was 0.12% with the Be target and 0.16% with the Ta target, which would correspond for the ^{15}C breakup to 6.7 MeV/c and 9.0 MeV/c for Be and Ta respectively.

The beam intensity was monitored by a set of small silicon detectors located near the production target. The ratio between the number of incoming nuclei of interest and the beam monitors was measured by transmitting the secondary beam directly to the focal plane. This ratio was later used to determine the breakup cross-sections.

4. Results and discussion

As can be seen in table 1, ^{15}C and ^{14}B are the two most well know nuclei of our study set. The angular distribution from the ground state of ^{15}C in the reaction ^{14}C(d,p)^{15}C [8] reveal that it is a 1/2$^+$. The set of optical parameters giving the best fit in a DWBA calculation also gives a spectroscopic factor of 0.88. This spectroscopic factor is in line with shell model calculations. The inversion of the $0d_{5/2}$ and $1s_{1/2}$ orbits results from a smaller kinetic energy of the neutrons in the $1s_{1/2}$ than in the $0d_{5/2}$ [19]. This ultimately comes from the neutron potential becoming shallower as the number of protons decreases, resulting from having less neutron-proton interactions. The ground state of ^{14}B is 2$^-$, resulting from a hole in the $0p_{3/2}$ proton shell and a single neutron in the $1s_{1/2}$ neutron shell. The neutron shell structure of ^{14}B is therefore very similar to that of ^{15}C, and a shell model calculation yields a spectroscopic factor of 0.95.

The parallel momentum distributions of ^{14}C and ^{13}B after the breakup of ^{15}C and ^{14}B on the Be target are presented in the top parts of figure 1. The momentum distribution from ^{14}B breakup is shifted towards higher momenta because it was observed at Bρ values set on the center of the ^{17}C breakup, and the shift represents the difference in momentum between the two reactions. A fit to the data with a modified Lorentzian line-shape [10] is used to extract the experimental width (see also Table 2). The dashed lines shown in the spectra obtained for nuclear breakup come from an ℓ=0 Hankel function calculations with localization. A calculation using a Wood-Saxon potential gives very similar distributions. The effect of an eventual d-component in the wave function is negligible at the level of 10%, as it is the most supressed by the localization effect. Because the binding energies of ^{15}C and ^{14}B are well known, there is very little error on the calculated width. The horizontal error bar crossing the dashed curve represents the error due to the mass uncertainty, and is thinner than the line thickness on the figure.

It is apparent from figure 1 that the observed parallel momentum distributions from the one-neutron nuclear breakup of ^{15}C and ^{14}B are different from the predicted shapes. This comes as a surprise, since this calculation has been shown to reproduce the momentum distributions observed in the nuclear breakup of ^{11}Be and ^{8}B [9, 11]. In particular, the wave function of ^{11}Be is also known to be an almost pure s-state, although with a different binding energy. The main discrepancy with the calculation is found in the tails of the momentum distributions, which correspond to smaller radii in spacial coordinates. A

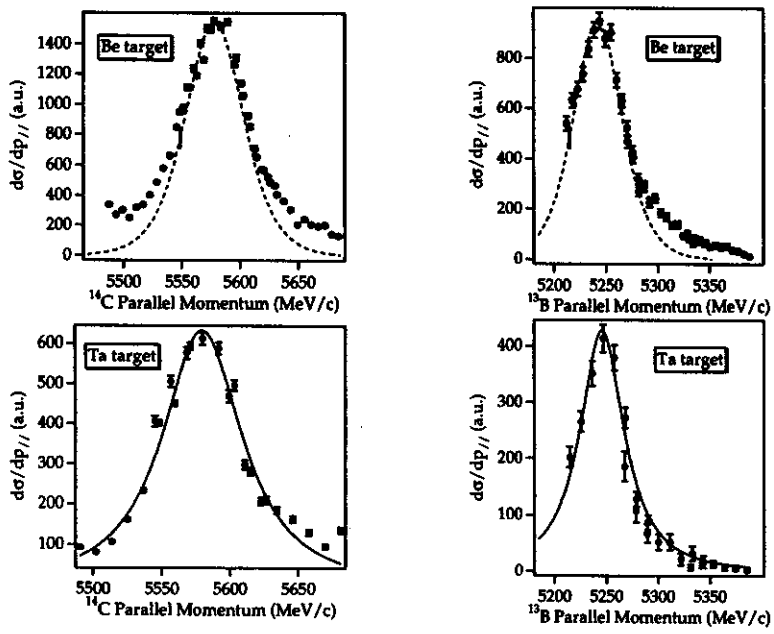

Figure 1: Left: parallel momentum distribution of ^{14}C after the breakup of ^{15}C on Be target (top) and Ta target (bottom). The dashed line in the top figure corresponds to an ℓ=0 Hankel function calculation taking into account the localization effect. The solid line in the bottom figure is a fit using a Modified Lorentzian line-shape. Right: parallel momentum distribution of ^{13}B after the breakup of ^{14}B on Be target (top) and Ta target (bottom). The dashed line in the top figure also corresponds to an ℓ=0 Hankel function calculation taking into account the localization effect. The solid line in the bottom figure is a fit using a Modified Lorentzian line-shape.

closer look at figure 1 reveals that this discrepancy seems more pronounced for ^{15}C than for ^{14}B. These two facts suggest that the origin of the difference between the observations and the calculations lies in contributions from the core. As the binding energy increases, the extend of the halo decreases and breakup reactions where the core gets excited become possible. In a simple Yukawa model, the extend of the halo is inversely proportionnal to the square root of the binding energy: $\langle r^2 \rangle_{1/2} = \hbar/\sqrt{4\mu S_n}$ which gives halo radii of 3.03 fm and 3.40 fm as compared to core radii of 2.70 fm and 2.64 fm for ^{15}C and ^{14}B respectively. These numbers indicate that the halos of ^{15}C and ^{14}B are only 12% and 29% bigger in radius that their respective cores, which strongly suggest that core contributions are likely to play a role in the one- neutron breakup channel. As a comparison the halo of ^{11}Be calculated in the same manner is found to be 95% bigger in radius than its core. Calculations including these core contributions would be needed for a more realistic comparison with the data. Very recent data was taken on the breakup of ^{15}C with γ-rays detected in coincidence with the fragment. It suggests that a contribution where the ^{14}C fragment is excited to its first excited p-state at 6.09 MeV could account for the discrepancy observed in the tails of the distributions [21].

Nucleus	Be target	Calculated nuclear	Ta target
^{14}B	57 ± 2 MeV/c	50.4 ± 0.5 MeV/c	48 ± 3 MeV/c
^{15}C	67 ± 3 MeV/c	54.3 ± 0.02 MeV/c	67 ± 1 MeV/c
^{17}C	145 ± 5 MeV/c	133.3 ± 0.5 MeV/c	-
^{19}C	42 ± 4 MeV/c	51.6 ± 1.6 MeV/c	41 ± 3 MeV/c

Table 2: Measured and calculated FHWM of the parallel momentum distributions expressed in the c.m. system. The experimental values are based on a fit to the data by a modified Lorentzian line-shape. The calculated values correspond to the calculation which reproduces the data the best (see text).

The bottom parts of figure 1 shows the parallel momentum distributions obtained in the one-

Because the d component is so weak and more suppressed by the localization effect than the s component, it can be neglected. The momentum distribution calculated using a Wood-Saxon potential is displayed on top the data in fig. 3 and is in better agreement than the calculation assuming a $1/2^+$ ground state. Due to the larger separation energy, the width of the parallel momentum distribution is much less sensitive to the mass determination of ^{19}C, as indicated by the error bar. The comparison of cross sections calculated with either an s-state coupled to the 0^+ ground state or the 2^+ state of ^{18}C leads to the same conclusion. The first calculation yields 290 mb and the second 84 mb, compared to the experimental value of 105 ± 17 mb (see also Table 3). The same result is also suggested by recent coupled channel calculations performed using a deformed Wood-Saxon potential [18].

The parallel momentum distribution of ^{18}C from the Coulomb breakup of ^{19}C on a Ta target is displayed on the bottom of fig. 3. The observed width is very similar to the nuclear breakup width, wih a modified-Lorentzian fit yielding a FWHM of 41 ± 3 MeV/c. This width is in agreement with the results from a recent experiment [14] where neutrons from the breakup of ^{19}C have been observed.

5. Conclusion

In this experiment, we have measured the longitudinal momentum of core fragments emmited from the one-neutron breakup of the following nuclei: ^{14}B, ^{15}C, ^{17}C and ^{19}C. Both nuclear and Coulomb dissociations were investigated using Be and Ta targets, except in the Coulomb dissociation of ^{17}C for which the background could not be removed. This set of nuclei was chosen because of the various binding energies and angular momenta of their ground states, in an attempt to explore the circumstances of formation of halos. The two nuclei ^{14}B and ^{15}C provide good test cases for the appearance of halos, as their wave functions and binding energies are well known. However, a clear discrepancy with the calculations is observed. This discrepancy is being interpreted as core contributions in the nuclear breakup, in which channels leading to the excitation of the core are being opened as the size of the halo is reduced, due to a relatively large binding energy.

The broad parallel momentum distribution obtained from the one-neutron nuclear breakup of ^{17}C shows no halo formation in this nucleus. With a separation energy of 0.73 MeV, this suggests a halo suppression due to the centrifugal barrier. Indeed, the spin-parity of the ^{17}C ground state is not well established, and shell model calculations indicate a very close proximity between the $1s_{1/2}$ and $0d_{5/2}$ orbits. A calculation using parentage coefficients obtained from the shell model gives the best agreement with the data for spin-parity of $3/2^+$ coupled to the first 2^+ excited state of ^{16}C. However, this agreement is still quite loose due to the large error bars on the data. Clearly better statistics would desirable in order to distinguish the shape of the parallel momentum distribution and make a more sensible comparison to the calculations.

With our previous measurement on the nuclear breakup of ^{19}C on Be target [2], this experiment completed the preliminary program by observing its one- neutron Coulomb breakup on a Ta target. The observed width is very similar in both breakup processes. The analysis of this data is complicated by the large uncertainty on the mass of this nucleus, and further experimental progress in that direction would be greatly beneficial. Like in the case of ^{17}C, the ground state properties of ^{19}C are not well known, and shell model predictions vary from one interaction to another. The nuclear breakup data does not seem to be consistant with a s-ground state coupled to the ground state of ^{18}C. Rather, an ℓ=0 ground state coupled to the first 2^+ excited state of ^{18}C seems to give the best agreement with the data, although a large leeway is allowed by the large error bars on both calculations and data. The principal difficulty in improving the

data on ^{19}C is the very small production rate. With the now commissioned new S800 spectrograph at the NSCL, we should be able to improve substancially the intensity and purity of the ^{19}C secondary beam, by using the S800 analysis line which has greater acceptances than the A1200 used in this experiment. This will also eliminate all acceptance cuts in the reaction cross section due to the large acceptance S800 spectrograph, as well as obtain information on the transverse momentum distributions.

a. Present address: Department of Physics, Allegheny College, Meadville, PA 16335
b. Present address: Department of Physics, Florida State University, Tallahassee, FL 32306

References

1. D. Bazin. *To be published*, 1997.
2. D. Bazin, B.A. Brown, J. Brown, M. Fauerbach, H. Hellström, S.E. Hirzebruch, J.H. Kelley, R.A. Kryger, D.J. Morrissey, R. Pfaff, C.F. Powell, B.M. Sherrill, and M. Thoennessen. *Phys. Rev. Lett.*, 74:3569, 1995.
3. C. A. Bertulani and G. Baur. *Nucl. Phys.*, A480:615, 1988.
4. C. A. Bertulani and K.W. McVoy. *Phys. Rev. C*, 46:2638, 1992.
5. B. A. Brown. *Private communication*, 1997.
6. B. L. Cohen. *Rev. Sci. Instrum.*, 30:415, 1959.
7. L. K. Fifield, J. L. Durell, M. A. C. Hotchkis, J. R. Leigh, T. R. Ophel, and D. C. Weisser. *Nucl. Phys.*, A385:505, 1982.
8. J.D. Goss, A.A. Rollefson, C.P. Browne, R.A. Blue, and H.R. Weller. *Phys. Rev. C*, 8:514, 1973.
9. P.G. Hansen. *Phys. Rev. Lett.*, 77:1016, 1996.
10. J. H. Kelley, Sam M. Austin, D. Bazin, T. Kubo, and B. M. Sherrill. *Nucl. Instrm. and Meth. in Phys. Res.*, A386:492, 1997.
11. J.H. Kelley, S.M. Austin, A. Azhari, D. Bazin, J.A. Brown, H. Esbensen, M. Fauerbach, M. Hellström, S.E. Hirzebruch, R. A. Kryger, D.J. Morrissey, R. Pfaff, C.F. Powell, E. Ramakrishnan, B.M. Sherrill, M. Steiner, T. Suomijärvi, and M. Thoennessen. *Phys. Rev. Lett.*, 77:5020, 1996.
12. T. Kobayashi, O. Yamakawa, K. Omata, K. Sugimoto, T. Shimoda, N. Takahashi, and I. Tanihata. *Phys. Rev. Lett.*, 60:2599, 1988.
13. B. Lohmann and E. Weingold. *Phys. Lett. A*, 86:139, 1981.
14. F. M. Marqués, E. Liegard, N. A. Orr, J. C. Angélique, L. Axelsson, G. Bizard, W. N. Catford, N. M. Clarke, G. Costa, M. Freer, S. Grévy, D. Guillemaud-Mueller, G. J. Gyapong, F. Hanappe, P. G. Hansen, B. Heusch, B. Jonson, C. Le Brun, F. R. Lecolley, F. Lefebvres, M. Lewitowicz, G. Martínez, A. C. Mueller, T. Nilsson, A. Ninane, G. Nyman, B. Petersen, F. Pougheon, K. Riisager, M. G. Saint-Laurent, Y. Schutz, M. Smedberg, O. Sorlin, L. Stuttgé, and D. D. Warner. *Phys. Lett. B*, 381:407, 1996.
15. N.A. Orr, N. Anantaraman, S.A. Austin, C.A. Bertulani, K. Hanold, J.H. Kelley, R.A. Kryger, D.J Morrissey, B.M. Sherrill, G.A. Souliotis, M. Steiner, M. Thoennessen, J.S. Winfield, J.A. Winger, and B.M. Young. *Phys. Rev. C*, 51:3116, 1995.
16. A. Ozawa, G. Raimann, R. N. Boyd, F. R. Chloupek, M. Fujimaki, K. Kimura, H. Kitagawa, T. Kobayashi, J. J. Kolata, S. Kubono, I. Tanihata, Y. Watanabe, and K. Yoshida. *Nucl. Phys.*, A592:244, 1992.
17. Z. Ren, Z.Y. Zhu, Y.H. Cai, and G. Xu. *Nucl. Phys. A*, 605:75, 1996.
18. D. Ridikas, M. H. Smedberg, J. S. Vaagen, and M. V. Zhukov. *Europhys. Lett.*, 37:385, 1997.
19. H. Sagawa, B. A. Brown, and H. Esbensen. *Phys. Lett. B*, 309:1, 1993.
20. R. Serber. *Phys. Rev.*, 72:1008, 1947.
21. B. M. Sherrill. *To be published*, 1997.
22. B. M. Sherrill, D. J. Morrissey, J. A. Nolen Jr., and J. A. Winger. *Nucl. Instrm. Methods Phys. Res.,Sect. B*, 56&57:1106, 1991.
23. E. K. Warburton and B. A. Brown. *Phys. Rev. C*, 46:923, 1992.

MEASUREMENT OF THE REACTION CROSS SECTION OF d(^{7}Be,^{8}B)n

C. F. Powell, D. J. Morrissey, D. Anthony, B. Davids, M. Fauerbach,
P. F. Mantica, B. M. Sherrill, and M. Steiner

A large amount of study has been performed to determine the structure of the exotic nucleus ^{8}B. In particular, the possible existence of a single-proton halo in this nucleus has been suggested. Numerous experiments have been performed with ^{8}B, including measurements of total interaction cross section [1], quadropole moment [2], quasielastic scattering cross section [3], and momentum distributions of the breakup fragments [4]. These studies have reached conflicting conclusions about the existence of a proton halo. We performed NSCL Experiment 96019 in order to probe the structure of 8B using a different approach: the measurement of the d(^{7}Be,^{8}B)n reaction cross section and ultimately the determination of the spectroscopic factor for the ground state of ^{8}B.

In order to measure the (d,n) cross section of a reaction involving short-lived isotopes, it is necessary to use inverse kinematics. The NSCL is ideally suited for studies of this type because the A1200 radioactive beam facility can produce intense beams of exotic nuclei. Also, the existence of the NSCL Neutron Time-of-Flight array and a wide array of heavy ion detection equipment allows the measurement to be made with a minimum of detector development.

As this was the first measurement of its kind at the NSCL, it was important that a similar reaction which has been extensively studied also be measured as a proof-of technique. The comparison reaction chosen was d(^{12}C,^{13}N)n. This reaction is ideal because it is well-documented over a range of energies [5,6] and the relatively high energy of the first excited state of ^{13}N (2.37 MeV) should allow unambiguous separation of reactions leading to the ground state. Demonstration of the validity of the technique for the d(^{12}C,^{13}N)n reaction would thus substantiate the measurement of the cross section of d(^{7}Be,^{8}B)n.

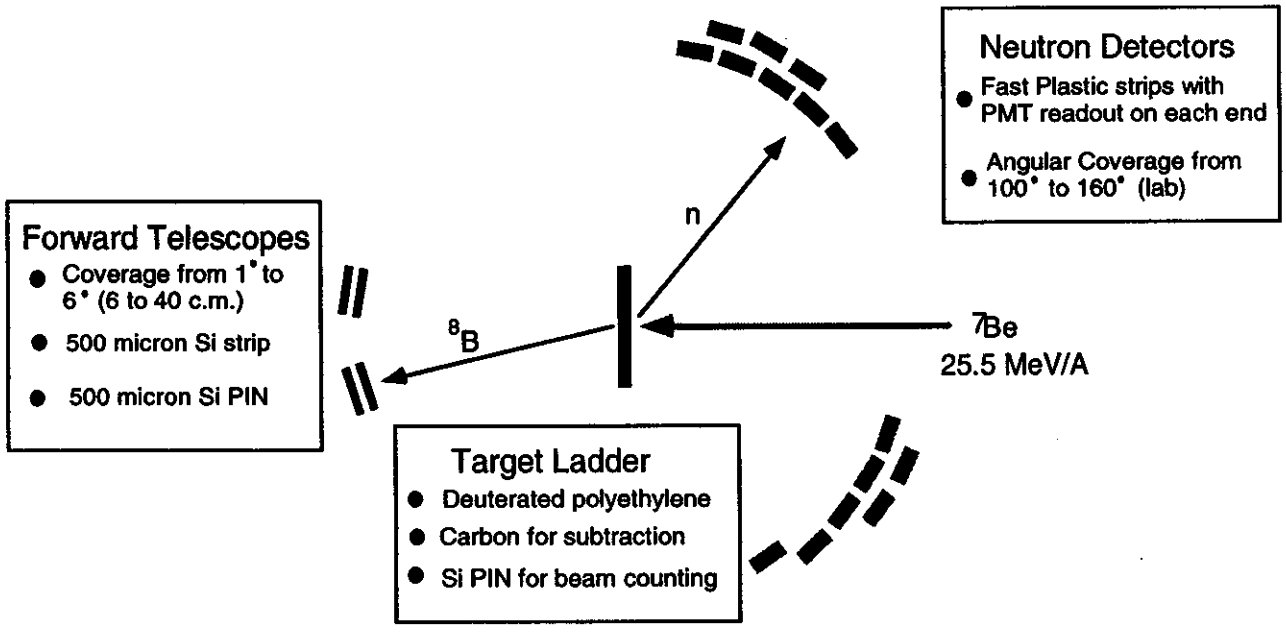

Figure 1: Side section of detectors for inverse kinematics measurement of the (d,n) cross sections.

The heavy ion beams used in the reaction studies were produced in the A1200 from a primary beam of $^{12}C^{3+}$ @ 60 MeV/A. 790 mg/cm^2 Be and 300 mg/cm^2 Al degraders were used to produce a beam of ^{12}C @ 22 MeV/A. A production target of 587 mg/cm^2 Be and a 300 mg/cm^2 Al wedge were subsequently used to produce the beam of ^7Be @ 25 MeV/A. This target-wedge combination gave a ^7Be rate of ~330,000 s^{-1} at the N3 target position with a primary beam current of ~130 pnA. The beam purity was greater than 95%.

The experiment was designed to measure the reaction cross sections of d(^{12}C,^{13}N)n and d(^7Be,^8B)n in inverse kinematics. Figure 1 shows a schematic diagram of the detectors used to make the measurements. The beam from the A1200 was focussed onto a deuterated polyethylene target. Position sensitive heavy-ion telescopes measured the angle and energy of the forward products, and the NSCL Neutron TOF array measured the angle and energy of the coincident neutrons emitted in the backward direction. The forward telescopes consisted of a silicon-strip detector for ΔE and position measurement, followed by a single-area PIN diode to measure total E. Energy resolution was ~400 keV FWHM, and the fragment angle was measured with a resolution better than 0.5° (center-of-mass). The neutron TOF array consisted of 16 plastic scintillator bars positioned ~1m from the target. These scintillators have PMTs at each end to measure position along the bar, while the neutron's time of flight gives its kinetic energy. The kinematic curves for the neutrons in coincidence with ^8B and the heavy fragments associated with these neutrons are shown in Figure 2, along with the measured kinematics from experiment 96019. The close agreement between the measurement and the kinematics demonstrate that we have definitely isolated the reaction of interest.

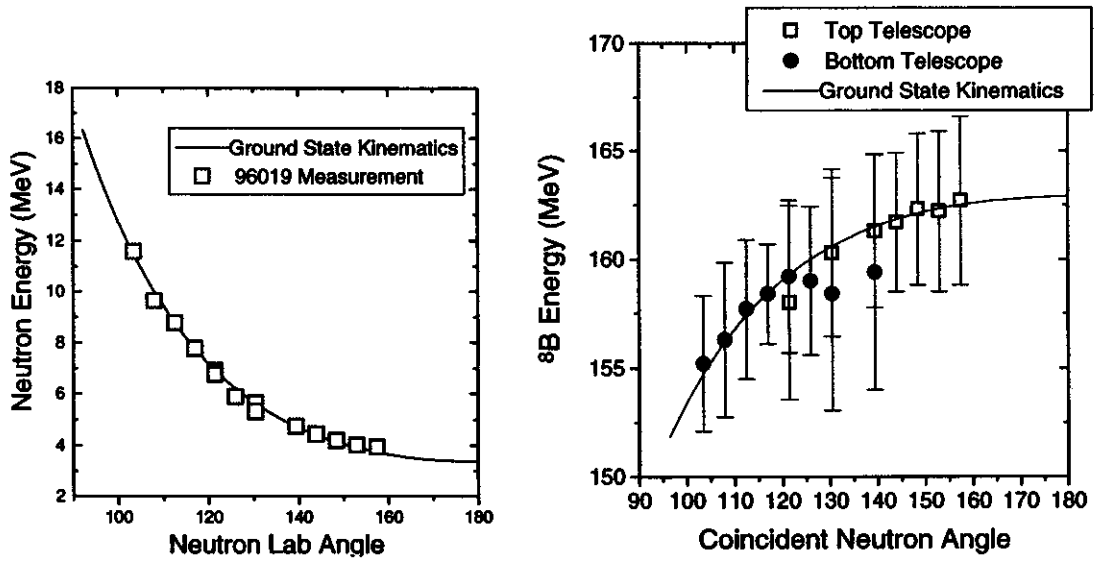

Figure 2: Kinematics of the d(^7Be,^8B)n reaction.

A figure containing the preliminary angular distribution of the cross section determined from the ^8B singles events is shown in Figure 3, along with a sample DWBA calculation. The coincidence neutron data is still under analysis. These cross section measurements, along with a more complete DWBA calculation, will be used to determine the spectroscopic factor for this reaction.

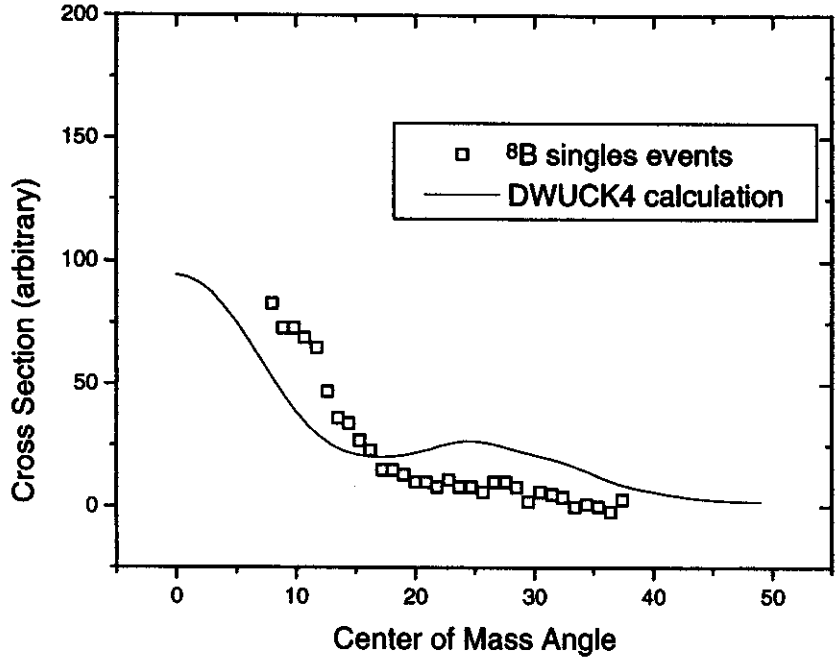

Figure 3: Measured reaction cross section and DWBA calculation using DWUCK4 [7].

References

1. I. Tanihata et al., *Phys. Lett.*, **B206** (1988) 592.
2. T. Minamisono et al., *Phys. Rev. Lett.*, **69** (1992) 2058.
3. I Pecina et al., *Phys. Rev. C*, **52** (1995) 191.
4. W. Schwab et al., *Z. Phys.*, **A350** (1995) 283.
5. H. R. Schelin et al., *Nucl. Phys.*, **A414** (1984) 67.
6. L. M. C. Dutton et al., *Nucl. Phys.*, **A178** (1972) 488.
7. Program DWUCK4, P. D. Kunz (unpublished), Extended version of J. R. Comfort (unpublished).

A MEASUREMENT OF THE $^{8}Li(n,\gamma)^{9}Li$ CROSS SECTION AT ASTROPHYSICAL ENERGIES BY REVERSE KINEMATICS

P. D. Zecher, A. Galonsky, S. Gaff, J. J. Kruse, G. Kunde, Erik Tryggestad, J. Wang, R. E. Warner, D. J. Morrissey, F. Deák[a], Á. Horváth[a], Á. Kiss[a],Z. Seres[b], K. Ieki[c], Y. Iwata[c], J. J. Kolata, J. von Schwartzenberg[d], and H. Schelin[e]

Reactions that bridge the mass-8 gap of instability are $\alpha + \alpha + \alpha \rightarrow {}^{12}C$ and $\alpha + \alpha + n \rightarrow {}^{9}Be$. $^{4}He(2n,\gamma)^{6}He(2n,\gamma)^{8}He(\beta^{-})^{8}Li$ followed by $^{8}Li(n,\gamma)^{9}Li$ is a possible set of bridging reactions in a neutron-rich environment. The importance of this bridge to heavier elements depends, among other things, on the value of the cross section for the $^{8}Li(n,\gamma)^{9}Li$ reaction. The primordial production of heavy elements will also depend on a knowledge of this cross section if the inhomogeneous model of the big bang is valid.

A number of theoretical estimates exist for the $^{8}Li(n,\gamma)^{9}Li$ cross section. Some of the estimates are based on microscopic model calculations of the ^{8}Li structure [1,2] others are estimates based on the systematics of similar nuclei. [3,4] These estimates vary by over an order of magnitude.

^{8}Li's half-life of less than 1 second makes a direct measurement of the capture cross section probably impossible. Fortunately, we can produce a beam of ^{9}Li nuclei, perform a measurement of the inverse reaction, $^{9}Li + \gamma \rightarrow {}^{8}Li + n$, and use the principle of detailed balance to deduce the cross section for the neutron capture reaction. The photons for the inverse reaction are obtained by passing the ^{9}Li through the virtual photon field near a high-Z nucleus such as Pb or U. The photodisintegration cross section is then related to the the radiative capture cross section by [5]

$$\sigma_{(n,\gamma)}\left({}^{8}\mathrm{Li}+n\rightarrow{}^{9}\mathrm{Li}+\gamma\right)=\frac{2(2j_{^{9}Li}+1)}{(2j_{^{8}Li}+1)(2j_{n}+1)}\frac{k_{\gamma}^{2}}{k^{2}}\sigma_{(\gamma,n)}({}^{9}\mathrm{Li}+\gamma\rightarrow{}^{8}\mathrm{Li}+n), \qquad (1)$$

where k is the wave number for the $^{8}Li+n$ channel, k_γ is the photon wave number, and j_{9Li}, j_{8Li}, and j_n are the appropriate spins.

The photodisintegration cross section $\sigma_{(\gamma,n)}$ can be determined from the measured differential coulomb excitation cross section $d\sigma/dE_\gamma$ as

$$\sigma_{(\gamma,n)}=\frac{E_\gamma}{n_{E1}}\frac{d\sigma}{dE_\gamma}, \qquad (3)$$

where E_γ is the virtual photon energy and n_{E1} is the virtual photon number for electric dipole photons, which is calculable. [6] Since we have no control over the energy of the absorbed photon, it is necessary to measure it for each event. We get this from

$$E_\gamma = E_x = E_d + S_n, \qquad (2)$$

where the decay energy E_d is the sum of the kinetic energies of the ^{8}Li fragment and the neutron and S_n = 4.05 MeV is the neutron separation energy of ^{9}Li. Hence, a complete kinematics measurement of the two reaction products is required.

We note that the virtual photons have a monotonically decreasing energy spectrum, and, with a minumum energy of 4.05 MeV, it is likely that nuclear dissociation will compete effectively with coulomb dissociation. Our planned procedure, therefore, was to measure the dissociation in both low-Z and high-Z targets. Neutron detection was done with the MSU Neutron Walls, [7] the first experiment with this detector. Unfortunately, we could get results only for the Pb and U targets. For each target the dissociation cross section was about 0.5 mb for decay energy interval 0.0- 0.5 MeV and likewise for 0.5-1.0 MeV.

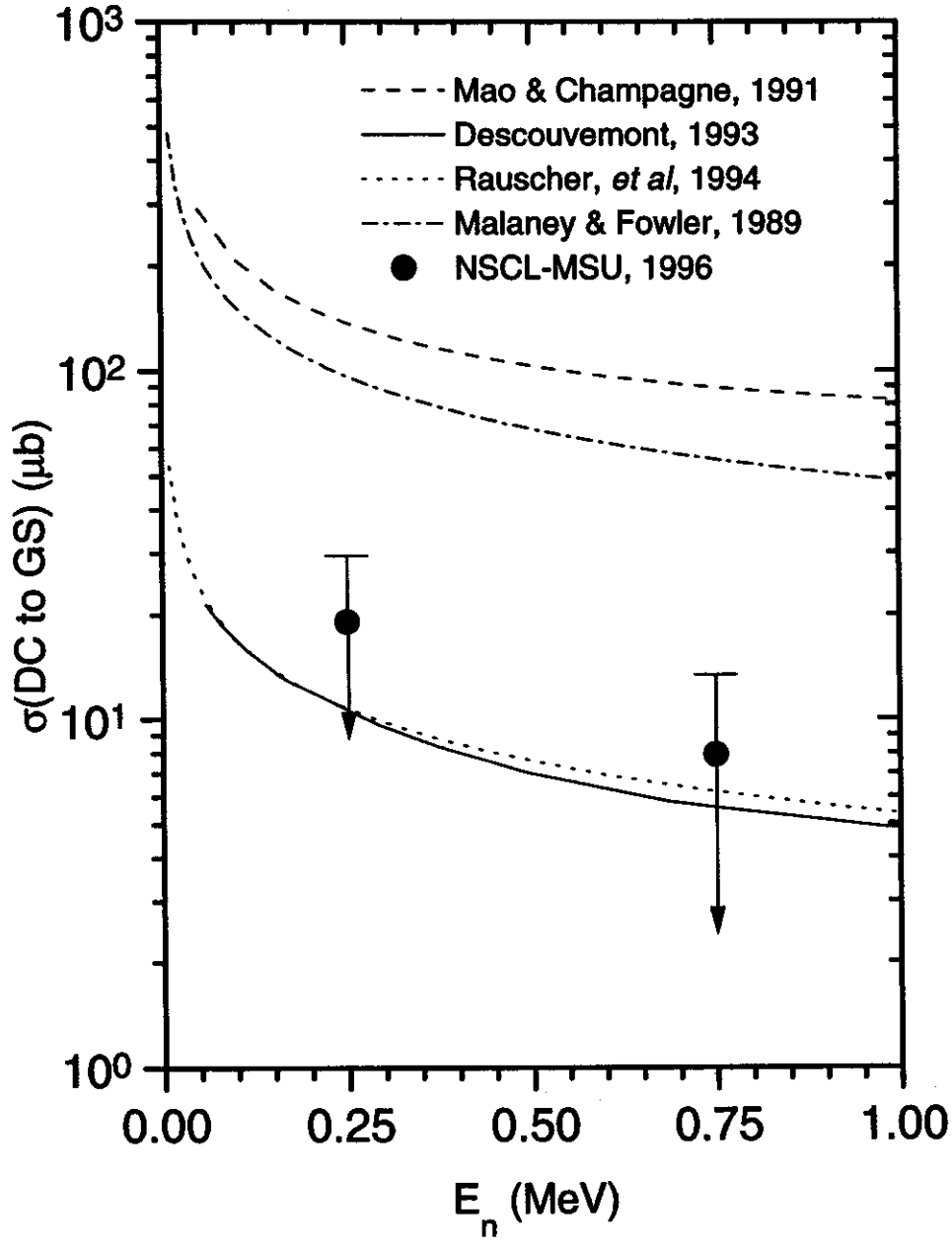

Radiative capture cross sections for ^{8}Li(n,γ)^{9}Li. The data points are upper limits measured using the coulomb dissociation method with a U target. All curves are for direct capture to the ground state, except that of Malaney & Fowler, which is for direct capture to the ground state plus first excited state.

Without results on the low-Z targets we have no way of determining how much of the cross section is photo produced, but surely our result gives an upper limit. Assuming that upper limit, we used Eqs. 1 and 2 to determine an upper limit to the (n,γ) cross section in the two energy intervals. The figure shows these values along with curves for the four predictions. We see that two, perhaps all four, of the predictions are inconsistent with our results. In the future we hope to do the experiment with enough beamtime to determine the dissociation on both high- and low-Z targets and thereby extract the actual coulomb part, not just an upper limit.

a. Department of Atomic Physics, Eötvös University, Puskin utca 5-7, H-1088 Budapest 8, Hungary
b. KFKI Research Institute for Particle and Nuclear Physics, 1525 Budapest 114 POB 49, Konkoly-These út 29-33, Hungary
c. Rikkyo University, 3 Nishi-Ikebukuro, Toshima, Tokyo 171, Japan
d. Department of Physics, University of Notre Dame, Notre Dame, Indiana 46556
e. CFET, Brazil

References

1. Z.Q. Mao and A.E. Champagne, Nucl.Phys. **A522**, 568 (1991)..
2. P. Decouvemont, Ap. J. **405**, 518 (1993).
3. T. Rauscher, J.H. Applegate, J.J. Cowan, F.K. Thielemann, and M. Wiescher, Ap.J. **429**, 499 (1994)..
4. R.A. Malaney and W.A. Fowler, Ap.J **333**, 14 (1988)..
5. R.G. Sachs, *Nuclear Theory* (Addison-Wesley Publishing Company, Inc., 1953), p. 141.
6. C. A. Bertulani and G. Baur, Physics Reports **163**, 302 (1988)..
7. P.D. Zecher et al., submitted to Nucl. Instr. & Meth.

SEARCH FOR DI-PROTON RADIOACTIVITY IN EXOTIC NUCLEI

P. G. Thirolf[a], A. Azhari, M. J. Chromik[a], T. Glasmacher, R. Ibbotson, R. A. Kryger, H. Scheit, M. Thoennessen, P. J. Woods[b], and S. Yokoyama

So far all experimental attempts to identify potential di-proton radioactivity at or near the proton dripline have failed (e.g. [1]). A promising candidate that has not yet been studied is ^{17}Ne, where the first excited state ($J^\pi = 3/2^-, E^* = 1.288$ MeV) is bound with respect to one-proton emission but unbound with respect to two-proton emission by 344 keV (for details see [2]). Therefore this state can only decay via two-proton decay to ^{15}O or γ-emission to the ground state of ^{17}Ne. In a recent intermediate energy Coulomb excitation experiment the γ-decay from the first excited state to the ground state ($J^\pi = 1/2^-$) has been measured for the first time and the experimental yield has been compared to the theoretically expected cross section. The measured γ-ray yield accounts only for 43% of the predicted yield from an excitation cross section of 18.7 mb, thus encouraging the investigation of a potential two-proton decay branch. However, if the missing cross section would decay via two-proton emission, the lifetime of this branch would be a factor 1700 smaller than predicted by standard barrier penetration calculations. The protons can either be emitted simultaneously but uncorrelated or via the emission of a di-proton (^{2}He configuration). This can only proceed to the ground state of ^{15}O, since the first excited state is at 5.18 MeV, well above the energy of ^{17}Ne. Moreover, the probability for a sequential decay through the ground state of ^{16}F is strongly hindered because it located 192 keV above the decay energy with a small width of $\approx$20 keV. Uncorrelated proton emission would lead to an isotropic angular distribution, while a significant angular correlation can be expected in case of the di-proton emission.

The experiment to search for this decay branch was performed at the NSCL using the technique of projectile fragmentation to produce the radioactive ^{17}Ne beam. A primary beam of ^{20}Ne at 100 MeV/u was used to bombard a 790 mg/cm^2 ^{9}Be production target. The fragmentation products were mass separated in the A1200 fragment separator, where an achromatic degrader wedge provided a first purification of the secondary beam, leading to a composition of 15% ^{17}Ne and 85% ^{15}O. Since the dominant beam contaminant is identical to the final nucleus of the two-proton decay of ^{17}Ne, a further purification was required. This was achieved with a Wien filter able to completely remove all unwanted ion species. As a result, 3000 ^{17}Ne particles per second were scattered off a 250 mg/cm^2 ^{197}Au target with an energy of 60 MeV/u.

A compact detector stack was positioned inside a beam tube with a diameter of 15 cm (Figure 1). A 40x40 double-sided silicon strip detector, a pin diode, a 5mm thick Si(Li) detector, a 16x16 double-sided silicon strip detector and a 4x4 CsI array were positioned in a close geometry at a distance of 16.3 cm behind the target. Thus 80% of the proton angular distribution could be observed from 0° to 7° (as obtained from Monte Carlo simulations of the two-proton decay) with an angular resolution of 0.35° per strip in the first detector. This 40x40 strip detector served to reconstruct the trajectories of the reaction products, while the subsequent pin diode (thickness 500μm, active area 5x5cm^2) provided the start signal for the trigger system. From both detectors an energy loss signal was derived and used for particle identification. The thickness of 5 mm of the following Si(Li) detector (diameter 5 cm) was chosen in a way to stop the heavy ^{15}O fragments completely, while protons would lose only about 20% of their initial energy. The 16x16 strip detector placed behind the Si(Li) allows to reconstruct the trajectories of the protons which then are stopped in the CsI array, consisting of 16 crystals, 1.7x1.7x5 cm^3 each, read out by pin diodes. In order to allow a simultaneous measurement of the proton decay and the γ-branch, a 38-element position sensitive

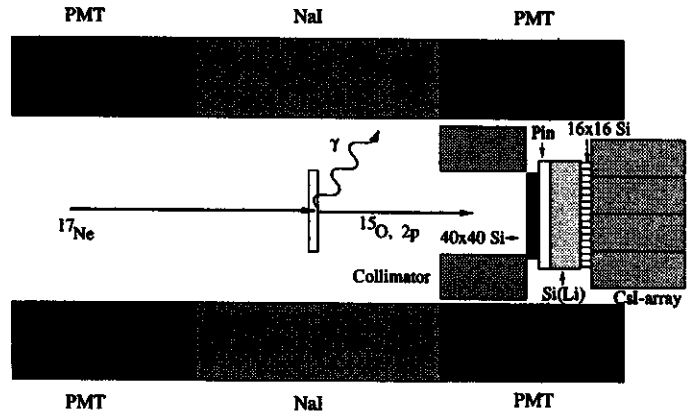

Figure 1: Setup for the simultaneous detection of the two-proton decay and the γ-decay of the first excited state in ^{17}Ne

NaI detector array was placed around the beam tube housing the target and the particle detector stack. A 6.5 cm thick lead collimator (with a central opening adapted to the size of the 40x40 strip detector) placed between target and detector stack shielded the NaI detectors from background γ-rays originating from the particle detectors.

Data were collected during 96 hours of beamtime and the offline analysis has just begun. Finally it should be noted that besides the possibility to investigate the potential two-proton decay from the first excited state in ^{17}Ne the data set obtained in the present experiment also allows to search for the ground state di-proton radioactivity in ^{16}Ne, though with reduced statistics.

a. Present address: Ludwig Maximilians Universität München, 85748 Garching, Germany.
b. The University of Edinburgh, Edinburgh EH9 3JZ, United Kingdom.

References

1. R. A. Kryger, A. Azhari, M. Hellström, J. H. Kelley, T. Kubo, R. Pfaff, E. Ramakrishnan, B. M. Sherrill, M. Thoennessen, S. Yokoyama, R. J. Charity, J. Dempsey, A. Kirov, N. Robertson, D. G. Sarantites, L. G. Sobotka, and J. A. Winger, Phys. Rev. Lett. 74, 860 (1995).
2. M. J. Chromik, B. A. Brown, M. Fauerbach, T. Glasmacher, R. Ibbotson, H. Scheit, P. Thirolf, and M. Thoennessen, Phys. Rev. C 55, 1676 (1997).